RSC Advances

PAPER

View Article Online
View Journal | View Issue

Check for updates

Cite this: *RSC Adv.*, 2020, **10**, 29642

Heteroleptic $Re(CO)_2^+$ and $Re(CO)_3^+$ complexes with α-diimines: similarities and differences in their luminescence properties

Andrzej Kapturkiewicz,* Anna Kamecka and Olga Grochowska

The photophysical properties of two series of phosphorescent rhenium(I) complexes, $[Re(CO)_2(N^N)(tpp)_2]^+$ and $[Re(CO)_3(N^N)(tpp)]^+$ with carbon monoxide (CO), triphenylphosphine (tpp) and α-diimine (N^N) ligands have been investigated in deoxygenated acetonitrile solution at room temperature and in solid methanol/ethanol 1 : 1 matrices at 77 K. The complexes display moderate to strong phosphorescence which is related to the N^N ligand modulated metal-to-ligand charge-transfer $S_0 \leftarrow {}^3$*MLCT or intraligand $S_0 \leftarrow {}^3$*LC transitions. Luminescence properties of the investigated series have been found to be very similar but some intrinsic differences between them are clearly seen. Whereas the $[Re(CO)_2(N^N)(tpp)_2]^+$ series shows MLCT emission in both temperature regimes studied, the $[Re(CO)_3(N^N)(tpp)]^+$ series exhibits intrinsic changes in its emission character when the measurement temperature is lowered from 298 to 77 K. In both investigated series, their emission characteristics are strongly affected by the nature of coordinated α-diimine N^N ligands. The observed trends, changes in the radiative k_r and non-radiative k_{nr} deactivation rate constants, have been compared with those found for the previously investigated $[Re(CO)_3(N^N)(Cl)]$, $[Re(CO)_3(N^N)(CH_3CN)]^+$, and $[Re(CO)_2(N^N)(dppv)]^+$ series (dppv = *cis*-1,2-bis(diphenylphosphino)-ethene). Similarities and differences in the spectroscopic and photophysical properties of five series of the $Re(CO)_3^+$ and $Re(CO)_2^+$ complexes have been analyzed in the view of results from DFT and TD-DFT computation and the emission band-shape analyses performed according to the Marcus–Jortner formalism.

Received 18th July 2020
Accepted 5th August 2020

DOI: 10.1039/d0ra06262f

rsc.li/rsc-advances

Open Access Article. Published on 11 August 2020. Downloaded on 7/22/2024 10:31:27 PM.
This article is licensed under a Creative Commons Attribution-NonCommercial 3.0 Unported Licence.

Introduction

Since the pioneering work of Wrighton and Morse on the luminescent $[Re(CO)_3(1,10\text{-phenathroline})(Cl)]$ molecule,[1] rhenium(I) complexes have occupied a prominent position in organometallic luminophores with a d^6 central metal ion.[2–4] Among these, the $[Re(CO)_3(N^N)(L)]^{0/+}$ chelates have attracted special attention due to their rich excited state behaviour that can be widely tuned by modification of the main N^N or ancillary L ligands and the medium or temperature.[5–12]

The photophysical properties of $[Re(CO)_3(N^N)(L)]^{0/+}$ species are governed by the relative energetic position and the interplay of the closely lying excited states of different characters. Particularly, the energy gaps between the excited ^{3}*LC (ligand centred) and ^{3}*MLCT (metal-to-ligand charge-transfer) triplet states are relatively small and allow efficient electronic interaction between them. The excited states of the *fac*-$Re(CO)_3^+$ complexes are mixed and their "real" excited states can be regarded as a superposition of the initial "pure" ^{3}*MLCT and ^{3}*LC components. This leads to monotonic changes in the nature of these emitters from the excited ^{3}*MLCT to ^{3}*LC character when appropriate changes of N^N and/or L ligands are involved. Consequently, the spectroscopic and photophysical properties of $[Re(CO)_3(N^N)(L)]^{0/+}$ complexes may be quite different, even for pretty similar N^N and/or L ligands present in their structures. This is because energies of the "pure" excited ^{3}*LC and ^{3}*MLCT states are affected in different ways.

The above-described behaviour is generally characteristic for many other transition metal complexes consisting d^6 ions and N^N ligands[13,14] including much less elaborated *cis*-$Re(CO)_2^+$ complexes[15–20] as well. The latter, containing monodentate PR_3 or bidentate P^P phosphines as ancillary ligands in their $[Re(CO)_2(N^N)(PR_3)_2]^+$ or $[Re(CO)_2(N^N)(P^P)]^+$ structures, are emissive in the spectral range consistent with the emission range observed for analogous $[Re(CO)_3(N^N)(Cl)]$ complexes. Their emissive properties, however, are noticeably better (higher quantum yields ϕ_{em} and longer lifetimes τ_{em} of emission) as compared to those found for their $[Re(CO)_3(N^N)(Cl)]$ analogues. Thus, the $Re(CO)_2^+$ based luminophores can be considered as very promising alternative in a wide range of applications in which the $Re(CO)_3^+$ chelates have been already applied. Among them, the most noticeable examples

Institute of Chemical Sciences, Siedlce University of Natural Sciences and Humanities, 3 Maja 54, 08-110 Siedlce, Poland. E-mail: andrzej.kapturkiewicz@uph.edu.pl; Tel: +48-25-643-10-97

This journal is © The Royal Society of Chemistry 2020

Open Access Article. Published on 11 August 2020. Downloaded on 7/22/2024 10:31:27 PM.
This article is licensed under a Creative Commons Attribution-NonCommercial 3.0 Unported Licence.

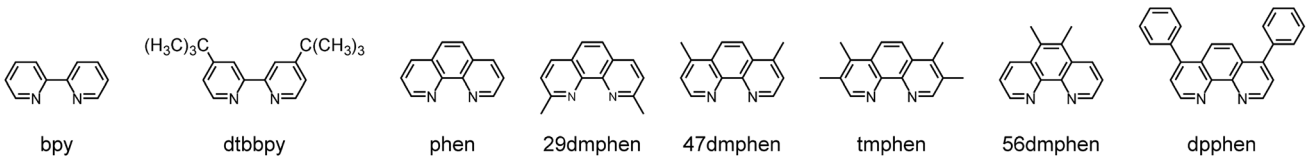

Fig. 1 Structures of N^N ligands investigated and their acronyms used in the text. 2,2′-Bipyridine – bpy, and 4,4′-di-*tert*-butyl-2,2′-bipyridyne – dtbbpy, 1,10-phenanthroline – phen, 2,9-dimethyl-1,10-phenanthroline – 29dmphen, 4,7-dimethyl-1,10-phenanthroline – 47dmphen, 3,4,7,8-tetramethyl-1,10-phenanthroline – tmphen, 5,6-dimethyl-1,10-phenanthroline – 56dmphen, and 4,7-diphenyl-1,10-phenathroline – dpphen, respectively.

include photocatalysis,[21–23] luminescent sensors,[24–26] organic light emitting devices[27] or dye-sensitized solar cell.[28]

Luminescence properties of the $[Re(CO)_2(N^N)(P^P)]^+$ series[20] bearing *cis*-1,2-bis(diphenylphosphino)-ethene – dppv and different α-diimines as P^P and N^N ligands, have been recently studied in more detail. It has been found that the radiative as well as nonradiative deactivation processes of the excited ^{3}*$[Re(CO)_2(N^N)(dppv)]^+$ states are considerably suppressed as compared to the ^{3}*$[Re(CO)_3(N^N)(Cl)]$ ones.[12] This results in longer τ_{em} values and, due to still more pronounced suppression of the nonradiative deactivation, in definitely higher quantum yields ϕ_{em}. The observed changes in the τ_{em} and ϕ_{em} values were found to be connected with lowering of the rate constants describing the radiative $k_r = \phi_{em}/\tau_{em}$ and nonradiative $k_{nr} = (1 - \phi_{em})/\tau_{em}$ deactivation of the excited ^{3}*MLCT states. This can be attributed to the presence of P^P ligand or/and smaller number of CO group (two instead of three) in the previously investigated $[Re(CO)_2(N^N)(dppv)]^+$ complexes. To clarify the occurring issue we have decided to perform a more systematic, comparative study of luminescent $Re(CO)_3^+$ and $Re(CO)_2^+$ complexes bearing different α-diimine N^N (*cf.* Fig. 1) and triphenylphosphine – tpp ligands. For the studies reported here, two series of Re(I) chelates, $[Re(CO)_3(N^N)(tpp)]^+$ and $[Re(CO)_2(N^N)(tpp)_2]^+$ were selected because their emission spectral ranges are expected matching these characteristic for their $[Re(CO)_2(N^N)(dppv)]^+$, $[Re(CO)_3(N^N)(Cl)]$ or $[Re(CO)_3(N^N)(CH_3CN)]^+$ analogues.[12,16,20]

Investigations reported in this paper are also devoted to the relationships between the nature of the given MLCT emitter and the k_r or k_{nr} rate constants characterizing the radiative and nonradiative $S_0 \leftarrow {}^3$*MLCT transitions in the α-diimine complexes. The experimentally observed huge variety in the k_r and k_{nr} values[16,20,29–31] are explainable by the N^N ligand induced changes in the electronic structure of these emitters from the ^{3}*MLCT to more pronounced ^{3}*LC character reflecting different mixing between the "pure" excited LC and MLCT configurations. Within this approximation, one can discuss the anticipated mixing taking into account the states energetically closest. In the simplest case, one can assume that the triplet ^{3}*MLCT configuration interacts with the lowest excited triplet state ^{3}*LC, typically localized within the N^N ligand. Due to the mixing between the "pure" ^{3}*MLCT and ^{3}*LC states, one can describe the resulting "real" emissive state as their superposition with the mixing coefficients c_{MLCT} and c_{LCT}

$$c_{MLCT}^2 = \frac{(E_{LCT} - E_{00})^2}{V_{33}^2 + (E_{LCT} - E_{00})^2} \quad \text{and} \qquad c_{LCT}^2 = \frac{V_{33}^2}{V_{33}^2 + (E_{LCT} - E_{00})^2} \tag{1}$$

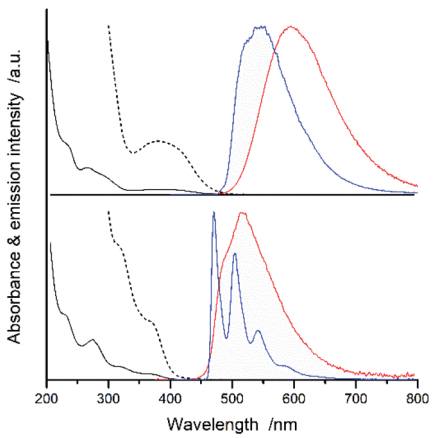

Fig. 2 Band profiles of the UV-vis absorption and emission spectra recorded for the $[Re(CO)_2(47dmphen)(tpp)_2]^+$ (top) and $[Re(CO)_3(47dmphen)(tpp)]^+$ (bottom) complexes. Room temperature absorption (black lines) in CH_3CN solutions. Room temperature (red lines) and 77 K (blue lines) emission in CH_3CN solutions and 1 : 1 CH_3OH/C_2H_5OH matrices, respectively. Dashed lines present expanded the low energy part of the UV-vis absorption.

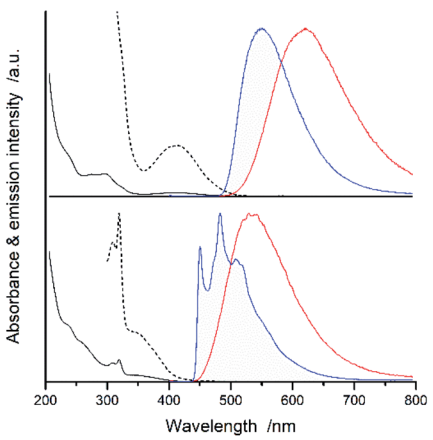

Fig. 3 Band profiles of the UV-vis absorption and emission spectra recorded for the $[Re(CO)_2(bpy)(tpp)_2]^+$ (top) and $[Re(CO)_3(bpy)(tpp)]^+$ (bottom) complexes. Room temperature absorption (black lines) in CH_3CN solutions. Room temperature (red lines) and 77 K (blue lines) emission in CH_3CN solutions and 1 : 1 CH_3OH/C_2H_5OH matrices, respectively. Dashed lines present expanded the low energy part of the UV-vis absorption.

Open Access Article. Published on 11 August 2020. Downloaded on 7/22/2024 10:31:27 PM.
This article is licensed under a Creative Commons Attribution-NonCommercial 3.0 Unported Licence.

where the V_{33} and $E_{LCT} - E_{00}$ are the electronic coupling element responsible for the interactions and the energy differences between the 0–0 transitions, the E_{LCT} and E_{00} values characterizing phosphorescence of the isolated N^N ligand and the complex, respectively. The latter quantity is affordable from the emission band-shape analysis.[31]

Despite of all its approximation, the LC/MLCT mixing approach seems to be applicable in any more quantitative discussion of the luminescent ^{3}*MLCT states including interpretation of the N^N ligand induced changes of the k_r and k_{nr} values. In the presented work, this has been tested for the $[Re(CO)_2(N^N)(tpp)_2]^+$ and $[Re(CO)_3(N^N)(tpp)]^+$ complexes. The obtained results have been compared with those previously obtained for the $[Re(CO)_3(N^N)(Cl)]$, $[Re(CO)_3(N^N)(CH_3CN)]^+$, and $[Re(CO)_2(N^N)(dppv)]^+$ complexes. Spectroscopic and photophysical properties of five series of the $Re(CO)_3^+$ and $Re(CO)_2^+$ complexes are discussed in the view of their emission band-shape analysis. This work presents also the results from DT and TD-DFT computation performed to clarify the observed similarities and differences.

Results and discussion

$S_0 \rightarrow {}^1$*MLCT absorption and $S_0 \leftarrow {}^3$*MLCT/^{3}LC emissions

Fig. 2 and 3 present examples of the room temperature absorption spectra of the studied complexes recorded in acetonitrile solutions. The spectra show superposition of the overlapping bands as characteristic for the transition metal complexes exhibiting typical MLCT features. Whereas, the high-energy bands can be ascribed to the $\pi \rightarrow \pi^*$ transitions localized within ligands attached to the central Re(I) core, the lowest energy bands with relatively low intensities can be attributed to the MLCT transitions. Generally, the spectra are very similar to those characterizing other Re(I) complexes with chelating α-diimine ligands. More specifically, the UV-vis spectra characterizing the studied $[Re(CO)_2(N^N)(tpp)_2]^+$ chelates correspond well to their $[Re(CO)_2(N^N)(dppv)]^+$ analogues,[20] whereas the $[Re(CO)_3(N^N)(tpp)]^+$ complexes exhibit features closer to that found for their $[Re(CO)_3(N^N)(CH_3CN)]^+$ counterparts.[12] This is reasonable because the spectrochemical parameters of tpp and CH_3CN ligands are very close one to another.[33] The same explanation holds for tpp and dppv ligands that explains resemblances between $[Re(CO)_3(N^N)(tpp)]^+$ and $[Re(CO)_2(N^N)(dppv)]^+$ series. Additionally, the positions of the CO and phosphine ligands in the spectrochemical series explain the observed bathochromic shift of the MLCT absorption and emission bands between the $Re(CO)_3^+$ and $Re(CO)_2^+$ complexes reported in this work (*cf.* data in Table 1).

Both series compared above are similar one to another in quantitative way as well. Although, due to the presence of the overlapping of many intra-ligand bands the high-energy parts of the recorded spectra are barely informative, one can draw some decisive conclusions comparing MLCT regions. Particularly, the overall MLCT intensities are very similar for the given N^N ligand and nearly independent of the remaining ligands attached to the central Re(I) ion (*cf.* Fig. 4). Fig. 4 presents data for the $[Re(CO)_2(N^N)(tpp)_2]^+$ and $[Re(CO)_3(N^N)(tpp)]^+$ series, but nearly the same relationship between the molar extinction coefficients ε_M is characteristic for $[Re(CO)_3(N^N)(Cl)]$ and $[Re(CO)_2(N^N)(dppv)]^+$ pair. Although the above examples concern complexes with sufficient separation of the MLCT and the intra-ligand absorption bands, similar situation seems to take place also for these α-diimine Re(I) complexes, $[Re(CO)_3(N^N)(CH_3CN)]^+$, where their MLCT bands are partly obscured by

Table 1 Spectroscopic and photophysical properties of $[Re(CO)_2(N^N)(tpp)_2]^+$ and $[Re(CO)_3(N^N)(tpp)]^+$ complexes (data in CH_3CN solutions at room temperature and methanol/ethanol 1 : 1 glasses at 77 K). Absorption maxima $\tilde{\nu}_{abs}^{max}$ and molar extinction coefficients ε_M of MLCT bands. Emission maxima $\tilde{\nu}_{em}^{max}$, emission quantum yields ϕ_{em}, and emission lifetimes τ_{em} of $S_0 \leftarrow T_1$ transitions

	Absorption at 298 K		Emission at 298 K			Emission at 77 K	
Ligand N^N	$\tilde{\nu}_{abs}^{max}$/ cm^{-1}	ε_M/ M^{-1} cm^{-1}	$\tilde{\nu}_{em}^{max}$/cm^{-1}	ϕ_{em}	τ_{em} / μs	$\tilde{\nu}_{em}^{max}$/cm^{-1}	τ_{em}/μs
$[Re(CO)_2(tmphen)(tpp)_2]^+$	27 050	5.6×10^3	17 100	0.52	21.6	18 450	38
$[Re(CO)_2(47dmphen)(tpp)_2]^+$	26 300	5.0×10^3	17 000	0.33	10.4	18 050	31
$[Re(CO)_2(29dmphen)(tpp)_2]^+$	25 000	2.7×10^3	15 950	0.045	0.43	17 600	7.5
$[Re(CO)_2(phen)(tpp)_2]^+$	27 050	3.8×10^3	16 150	0.20	4.6	17 800	22
$[Re(CO)_2(56dmphen)(tpp)_2]^+$	24 250	3.9×10^3	16 200	0.19	3.7	18 050	18
$[Re(CO)_2(dpphen)(tpp)_2]^+$	23 250	7.1×10^3	15 700	0.24	6.8	16 950	25
$[Re(CO)_2(dtbbpy)(tpp)_2]^+$	24 950	3.5×10^3	16 100	0.080	0.95	18 200	15
$[Re(CO)_2(bpy)(tpp)_2]^+$	24 250	2.8×10^3	15 950	0.042	0.63	17 950	15
$[Re(CO)_3(tmphen)(tpp)]^+$	27 050	2.8×10^3	20 550, 19 350	0.070	19.9	21 200, 19 750, 18 400, 16 950	480
$[Re(CO)_3(47dmphen)(tpp)]^+$	27 050	4.7×10^3	19 300	0.083	9.8	21 200, 19 850, 18 450, 17 100	430
$[Re(CO)_3(29dmphen)(tpp)]^+$	26 600	2.4×10^3	19 100	0.071	2.6	21 450, 20 250	41
$[Re(CO)_3(phen)(tpp)]^+$	27 050	3.3×10^3	18 800	0.088	2.3	21 600, 20 150, 18 800	42 (0.63), 156 (0.37)[a]
$[Re(CO)_3(56dmphen)(tpp)]^+$	25 850	3.1×10^3	19 800, 18 800	0.12	56	20 550, 19 200, 17 800	890
$[Re(CO)_3(dpphen)(tpp)]^+$	26 050	6.0×10^3	17 650	0.36	45	19 750, 18 550	70 (0.70), 160 (0.30)[a]
$[Re(CO)_3(dtbbpy)(tpp)]^+$	29 050	4.0×10^3	18 800	0.040	0.17	22 400, 21 150, 19 990	13
$[Re(CO)_3(bpy)(tpp)]^+$	28 750	3.5×10^3	18 400	0.040	0.29	22 200, 20 700, 19 500	8.6

[a] For $[Re(CO)_3(phen)(tpp)]^+$ and $[Re(CO)_3(dpphen)(tpp)]^+$ complexes bi-exponential emission decays were observed. Values given in parentheses are the normalized amplitudes of the short-lived and long-lived components of emission decays.

 This journal is © The Royal Society of Chemistry 2020

Open Access Article. Published on 11 August 2020. Downloaded on 7/22/2024 10:31:27 PM.
This article is licensed under a Creative Commons Attribution-NonCommercial 3.0 Unported Licence.

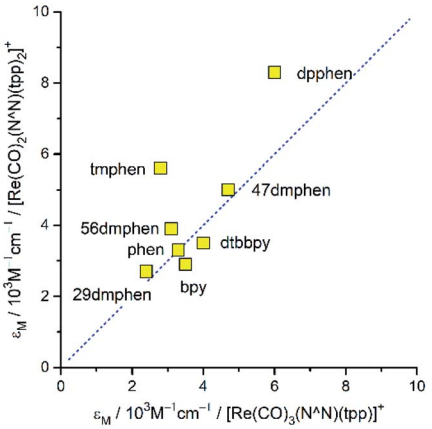

Fig. 4 Relation between the values of the molar extinction coefficients characterizing the MLCT band in the UV-vis absorption spectra of the $[Re(CO)_3(N^N)(tpp)]^+$) and $[Re(CO)_2(N^N)(tpp)_2]^+$ complexes in CH_3CN solutions. Experimental points are labelled with the N^N ligand abbreviations. The slope and intercept of the dashed line are equal to 1 and 0, respectively.

the intra-ligand absorption. Thus, one can emphasize very similar intensities of the MLCT absorption band as the characteristic feature of the $Re(CO)_3^+$ as well as $Re(CO)_2^+$ complexes.

Although, due to overlapping MLCT and LC bands, a quantitative characterization of the MLCT bands intensities is rather difficult, some estimates are possible taking into account the spectral positions $\tilde{\nu}_{abs}^{max}$ and spectral width $\Delta\tilde{\nu}_{1/2}$ of these bands. Using so-called the "lazy man's" approximation[34,35] one can approximately evaluate "effective" values of the transition dipole moments M_{abs} describing these bands from the respective extinction coefficient ε_M data. In nice accordance with the observed similar MLCT bands intensities, a quite small variation of the M_{abs} values is characteristic for the Re(I) complexes with α-diimine ligands. In most cases, the obtained M_{abs} values fall into the range of 1.5–2.5 D, somewhat larger $M_{abs} \sim 3.0$ D are characteristic only for the complexes with dpphen ligand. This finding implies nearly constant sum of oscillator strengths f of all $S_0 \rightarrow$ MLCT transitions potentially contributing to the MLCT bands of the discussed Re(I) complexes. One can rationalize the $\sum f =$ const claim assuming that the sum of the oscillator strength of the individual d $\rightarrow$ *π transitions ($d_{xy} \rightarrow$ *π, $d_{xz} \rightarrow$ *π, *etc.*) is constant as well. Then, independently how the given d orbital(s) will contribute to the occupied molecular orbitals involved in the transitions consisting the MLCT band (HOMO, HOMO−1, *etc.*), one can expect very similar values of its overall intensity. This expectation is also valid when the configuration interactions would be required for the proper description of the individual MLCT transitions. In the case of discussed Re(I) complexes it seems to be obvious that their UV-vis spectroscopic properties are connected with the presence of low energetically lying ^{1}*MLCT states. Results from the DFT and TD-DFT computations, performed for the ground state optimized geometries (*vide infra*), confirm this anticipation without any doubts.

All of the Re(I) complexes under study are luminescent both at room temperature and at 77 K. The luminescence spectra recorded for deaerated solutions in CH_3CN at 298 K are typically broad and, in most cases, show no vibronic structure. The spectral positions of the emission bands depend on the nature of the N^N ligand present in the structures of the studied $[Re(CO)_2(N^N)(tpp)_2]^+$ as well as $[Re(CO)_3(N^N)(tpp)]^+$ series (*cf.* data in Table 1). The observed trends in the emission maxima follow that expected for the $S_0 \leftarrow {}^3$*MLCT transitions taking into accounts changes in the electron withdrawing properties of the coordinated N^N ligand. These changes, caused by the presence of the methyl (electron donor) or the phenyl (electron acceptor) substituents attached to the parent phen or bpy ligands, lead to hypsochromic or bathochromic shifts of the emissions, respectively.

Intrinsic differences are, however, characteristic for the emission recorded at 77 K in the CH_3OH/C_2H_5OH matrices. The investigated $[Re(CO)_2(N^N)(tpp)_2]^+$ complexes exhibit broad and structureless bands. The observed hypsochromic shift allows concluding destabilization of the emissive ^{3}*MLCT states caused by hindered solvent/solute relaxation caused by the extreme viscosity of the low temperature glasses.[36,37] The studied $[Re(CO)_3(N^N)(tpp)]^+$ complexes demonstrate, however, distinctly different 77 K behaviour exhibiting nicely structured emission bands. Their positions and shapes resemble emissions from the isolated N^N ligands.[38–40] Thus, the observed rigidochromism can be related to the temperature induced changes in the nature of the emissive ^{3}*$[Re(CO)_3(N^N)(tpp)]^+$ species, from the excited ^{3}*MLCT to the excited intra-ligand ^{3}*LC.

Similarly, as it can be seen in the UV-vis absorption spectra, the emissive properties of the $[Re(CO)_2(N^N)(tpp)_2]^+$ and $[Re(CO)_3(N^N)(tpp)]^+$ complexes depend on the nature of the N^N ligand present in their structure. This is particularly true for the kinetic parameters associated with the radiative and non-radiative deactivations of the excited ^{3}*$[Re(CO)_2(N^N)(tpp)_2]^+$ and ^{3}*$[Re(CO)_3(N^N)(tpp)]^+$ species (*cf.* data in Table 2). The rate constants for these processes, determined from $k_r = \phi_{em}/\tau_{em}$ and $k_{nr} = (1 - \phi_{em})/\tau_{em}$ relationships, exhibit large diversity, much larger as compared to the variations of the ε_M values. This is also true for the transition dipole moments M_{em} of the $S_0 \leftarrow {}^3$*MLCT emissions as determined using the following relationship

$$k_r = (16\pi^3/3h\varepsilon_o)(n\tilde{\nu}_{em}^{max})^3|M_{em}|^2 \quad (2)$$

where n and ε_o denote the solvent refractive index and the vacuum permittivity. When the M_{abs} values depend marginally on the N^N ligand, the M_{em} values differ by almost one order of magnitude.

Analysing more deeply the room temperature data for the $[Re(CO)_2(N^N)(tpp)_2]^+$ and $[Re(CO)_3(N^N)(tpp)]^+$ complexes, one can see intrinsic correlation between the determined k_r and k_{nr} rate constants. Monotonic relationships between these rate constants (*cf.* Fig. 5) are characteristic for the excited triplet ^{3}*$[Re(CO)_2(N^N)(tpp)_2]^+$ and ^{3}*$[Re(CO)_3(N^N)(tpp)]^+$ states. Very likely, such behaviour, reported previously for other Re(I) complexes,[12,20] seems to be a general rule for the α-diimine

Open Access Article. Published on 11 August 2020. Downloaded on 7/22/2024 10:31:27 PM.
This article is licensed under a Creative Commons Attribution-NonCommercial 3.0 Unported Licence.

Table 2 Kinetic and energetic parameters characterizing $S_0 \leftarrow {}^3$*[Re(CO)$_2$(N^N)(tpp)$_2$]$^+$ and $S_0 \leftarrow {}^3$*[Re(CO)$_3$(N^N)(tpp)]$^+$ emissions (data in CH_3CN solutions at room temperature). Rate constants of nonradiative k_{nr} and radiative k_r deactivation processes, transition dipole moments M_{em} of $S_0 \leftarrow T_1$ transitions, and electronic coupling elements V_{30}. Fitted values of 0–0 transitions energies E_{00}, reorganization energies λ_{LM} and λ_H, and vibrational quanta $h\nu_H$

	Kinetic parameters				Energetic parameters (from band-shape analysis)				
Ligand N^N	k_{nr}/s^{-1}	k_r/s^{-1}	M_{em}/D	V_{30}/eV	E_{00}/eV	λ_{LM}/eV	λ_H/eV	$h\nu_H$/eV	k_{nr}/s^{-1} (calc)[a]
[Re(CO)$_2$(tmphen)(tpp)$_2$]$^+$	2.2×10^4	2.4×10^4	0.08	0.011	2.23	0.28	0.22	0.15	3.1×10^3
[Re(CO)$_2$(47dmphen)(tpp)$_2$]$^+$	6.4×10^4	3.2×10^4	0.09	0.013	2.20	0.31	0.20	0.17	7.1×10^4
[Re(CO)$_2$(29dmphen)(tpp)$_2$]$^+$	2.2×10^6	1.0×10^5	0.18	0.024	2.04	0.38	0.18	0.20	2.7×10^6
[Re(CO)$_2$(phen)(tpp)$_2$]$^+$	1.7×10^5	4.3×10^4	0.12	0.015	2.04	0.40	0.16	0.19	2.2×10^5
[Re(CO)$_2$(56dmphen)(tpp)$_2$]$^+$	2.2×10^5	5.1×10^4	0.13	0.017	2.07	0.37	0.17	0.18	1.3×10^5
[Re(CO)$_2$(dpphen)(tpp)$_2$]$^+$	1.1×10^5	3.5×10^4	0.11	0.014	2.00	0.35	0.18	0.17	1.6×10^5
[Re(CO)$_2$(dtbbpy)(tpp)$_2$]$^+$	9.7×10^5	8.4×10^4	0.16	0.022	2.08	0.41	0.20	0.18	1.0×10^6
[Re(CO)$_2$(bpy)(tpp)$_2$]$^+$	1.5×10^6	6.7×10^4	0.15	0.019	2.02	0.43	0.18	0.19	1.1×10^6
[Re(CO)$_3$(tmphen)(tpp)]$^+$	4.7×10^4	3.5×10^3	0.03	0.004	2.55	0.11	0.28	0.17	3.6×10^2
[Re(CO)$_3$(47dmphen)(tpp)]$^+$	9.4×10^4	8.5×10^3	0.04	0.006	2.53	0.12	0.30	0.16	9.5×10^2
[Re(CO)$_3$(29dmphen)(tpp)]$^+$	3.6×10^5	2.7×10^4	0.07	0.011	2.41	0.38	0.20	0.22	7.1×10^4
[Re(CO)$_3$(phen)(tpp)]$^+$	4.0×10^5	3.8×10^4	0.09	0.014	2.37	0.38	0.20	0.23	3.3×10^5
[Re(CO)$_3$(56dmphen)(tpp)]$^+$	1.6×10^4	2.1×10^3	0.02	0.003	2.47	0.12	0.25	0.17	1.6×10^2
[Re(CO)$_3$(dpphen)(tpp)]$^+$	1.4×10^4	8.0×10^3	0.04	0.006	2.33	0.19	0.28	0.17	1.9×10^4
[Re(CO)$_3$(dtbbpy)(tpp)]$^+$	5.6×10^6	2.4×10^5	0.22	0.036	2.39	0.42	0.24	0.22	5.3×10^6
[Re(CO)$_3$(bpy)(tpp)]$^+$	3.3×10^6	1.4×10^5	0.17	0.025	2.35	0.43	0.23	0.22	2.8×10^6

[a] k_{nr} values calculated using E_{00}, λ_{LM}, λ_H, and $h\nu_H$ parameters from performed emission band-shape analyses and V_{30} values as estimated using the Hush–Mulliken relationship $V_{30} = hc\tilde{\nu}_{em}^{max} M_{em}/\Delta\mu$.

chelates of $Re(CO)_3^+$ and $Re(CO)_2^+$ ions. Although the experimental points are somewhat scattered, the found coincidences between k_{nr} and k_r values allow concluding that all three discussed series of the $Re(CO)_3^+$ complexes (with tpp, CH_3CN, and Cl^- ancillary ligands) are very similar to each other. In an analogous way, one can also postulate close analogy between two [Re(CO)$_2$(N^N)(tpp)$_2$]$^+$ and [Re(CO)$_2$(N^N)(dppv)]$^+$ series.

Band-shape analysis of the $S_0 \leftarrow {}^3$*MLCT emission spectra

The observed k_r *vs.* k_{nr} relations point to noticeable association between the radiative and non-radiative $S_0 \leftarrow {}^3$*MLCT processes as specific for the discussed Re(I) complexes. This finding remains consistent with that expected from close relation between the thermal and optical charge-transfers occurring in so-called inverted Marcus region where these processes are bound one to another. Pursuing the close analogy between them, one can relate their kinetic description to the same set of the energetic parameters associated with the radiative and nonradiative $S_0 \leftarrow {}^3$*MLCT transition.

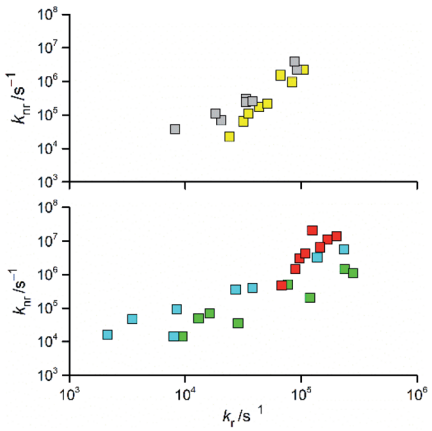

Fig. 5 Relations between the values of k_r and k_{nr} rate constants for the $Re(CO)_2^+$ (top) and $Re(CO)_3^+$ (bottom) complexes. Data for [Re(CO)$_2$(N^N)(tpp)$_2$]$^+$ (yellow symbols), [Re(CO)$_2$(N^N)(dppv)]$^+$ (grey symbols),[20], [Re(CO)$_3$(N^N)(tpp)]$^+$ (cyan symbols), [Re(CO)$_3$(N^N)(CH_3CN)]$^+$ (green symbols),[12] and [Re(CO)$_3$(N^N)(Cl)] (red symbols)[12] complexes in CH_3CN solutions at room temperature.

For more quantitative description of these processes one can use a commonly accepted formalism introduced by Marcus[41–43] and developed further by many other authors.[44,45] A moderately simple approach, based on the separation of low frequency λ_L, medium frequency λ_M and high frequency λ_H reorganization energies allows the description of the charge-transfer emission profile, *i.e.*, the emission intensity $I(\tilde{\nu}_{em})$ *vs.* the emitted photon energy $hc\tilde{\nu}_{em}$. In the case of the transition metal complexes exhibiting the MLCT emission, the λ_M and λ_H energies are mainly connected with changes of the intra-ligand and the ligand–metal bonds, whereas the λ_L energy is mostly associated with the solvent shell reorganization. When the semi-classical treatment of the medium-frequency modes together with the classical and quantum treatment of the low frequency and the high frequency modes are applied,[32,46] the following expression can be obtained

$$\frac{I(\tilde{\nu}_{em})}{(n\tilde{\nu}_{em})^3} = \frac{64\pi^4}{3h} M_{em}{}^2 \sum_{j=0} \frac{e^{-S} S^j}{j!} \exp\left[- \frac{(E_{00} - jh\nu_H - hc\tilde{\nu}_{em})^2}{4\lambda_{LM} k_B T} \right] \quad (3)$$

This journal is © The Royal Society of Chemistry 2020

Open Access Article. Published on 11 August 2020. Downloaded on 7/22/2024 10:31:27 PM.
This article is licensed under a Creative Commons Attribution-NonCommercial 3.0 Unported Licence.

where E_{00}, $h\nu_H$, k_B and T are the energy of the 0–0 transitions, the average spacing of the quantized high frequency intra-molecular modes undergoing reorganization upon charge-transfer, the Boltzmann constant, and absolute temperature, respectively. Parameter S in eqn (3) corresponds to the electron-vibrational coupling constant defined as $S = \lambda_H/h\nu_H$.

Within the same framework, the values of k_{nr} rate constants are predictable from the following expression[29,47,48]

$$k_{nr} = \frac{4\pi^2}{h}\frac{{V_{30}}^2}{\sqrt{4\pi\lambda_{LM}k_BT}}\sum_{j=0}\frac{e^{-S}S^j}{j!}\exp\left[-\frac{(E_{00}-jh\nu_H)^2}{4\lambda_{LM}k_BT}\right] \quad (4)$$

where V_{30} is related to an effective electronic coupling matrix element describing electronic interactions between the S_0 and ^{3}*MLCT states participating in the non-radiative $S_0 \leftarrow {}^3$*MLCT thermal charge-transfer.

The λ_{LM} term present in eqn (3) and (4), contain contributions from the low frequency (treated classically) and medium frequency (treated semi-classically) reorganization energies. Within these assumptions, one can approximate the resulting effective λ_{LM} value as follows[32,48]

$$\lambda_{LM} = \lambda_L + \lambda_M(h\nu_M/2k_BT)\coth(h\nu_M/2k_BT) \quad (5)$$

where $h\nu_M$ corresponds to the average spacing of the quantized medium frequency intra-molecular vibrations participating in the $S_0 \leftarrow {}^3$*MLCT transitions.

Representative examples of the numerical fits, presented in Fig. 6, show that, despite all approximations of the single frequency model applied, one can reproduce quite well the experimental emission profiles of the studied complexes. Emission spectra of the complexes under investigations were fitted by the application of a one-mode Franck–Condon analysis according to eqn (3) with the quantities relevant for their radiative charge-transfer (*i.e.*, E_{00}, λ_{LM}, λ_H, and $h\nu_H$ summarized in Table 2) varied as free fit parameters. It should be noted, however, that the fitted quantities turn out to be somewhat correlated. This leads to numerical uncertainty (±0.02 eV) of their fitted values. Due to approximate character of the applied model, the real uncertainty of the fitted parameters can be slightly larger. Despite that, the obtained energetic quantities give somewhat deeper insight into the nature of the emissive ^{3}*MLCT species.

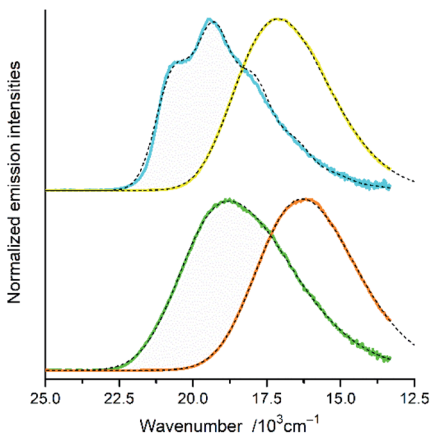

Fig. 6 Band profiles of the emission spectra recorded for the $[Re(CO)_2(tmphen)(tpp)_2]^+$ (yellow line), $[Re(CO)_2(dtbbpy)(tpp)_2]^+$ (orange line), $[Re(CO)_3(tmphen)(tpp)]^+$ (cyan lines), and $[Re(CO)_3(dtbbpy)(tpp)_2]^+$ (green line), complexes in CH_3CN solutions at room temperature. Dashed black lines correspond to the numerical fits according to eqn (5).

In the fitting procedure as used in this work, the applied classical, semi-classical and quantum-mechanical treatment of the low, medium and high frequency modes seems to be justified in the cases of 298 K emissions. One can additionally check this anticipation because the same set of parameters is, according to eqn (4), related to the rate constants of the non-radiative $S_0 \leftarrow {}^3$*MLCT transitions. Thus, one can additionally test the data from band-shape analyses by comparing the experimentally found rate constants k_{nr} with those calculated using eqn (4). Such calculations are possible because one can deduce the required V_{30} values from the experimentally available values of the MLCT emission maxima $\tilde{\nu}_{em}^{max}$ and the transition dipole moments M_{em}. Without going into details of the interaction between the coupled S_0 and ^{3}*MLCT states, one can estimate the V_{30} values using the Mulliken–Hush relationship[49–52]

$$M_{em} = \frac{V_{30}}{hc\tilde{\nu}_{em}^{max}}\Delta\mu \quad (6)$$

In the case of the discussed Re(I) complexes, one can approximate required $\Delta\mu$ value assuming the whole electron transfer over the distance between the central Re(I) ion and the centre of N^N ligands. Within this approach, one can obtain $\Delta\mu = 15$ D. Similarly, as it was done in our previous works, this quite reasonable value[53,54] was used for estimation of the V_{30} terms. The obtained V_{30} values together with the resulted k_{nr} rate constants are collected in Table 2. The agreement between the experimentally found and calculated rate constants k_{nr} is more than satisfactory for nearly all Re(I) complexes discussed in this work (*cf.* Fig. 7). In these cases, the discrepancies between the experimentally found and computed values do not exceed a factor of 3–4.

For some of the $[Re(CO)_3(N^N)(tpp)]^+$ complexes (with 47dmphen, 56dmphen, and tmphen ligands) one can see, however, significant discrepancy between the calculated and experimentally found k_{nr} values. In the case of these complexes, their largest E_{00} values may suggest the presence of an additional, thermally activated non-radiative deactivation channel. More specifically, the presence of the excited metal-centred ^{3}*MC state, often contributing to the non-radiative deactivation,[55,56] might be operative. However, one can eliminate this option because the expected energy splitting of the Re(I) d and *d orbitals as high as *ca.* 4 eV can be estimated using the spectrochemical parameters of the ligand present in the $[Re(CO)_3(N^N)(tpp)]^+$ complexes. This precludes possible ^{3}*MLCT → ^{3}*MC → S_0 deactivation path due to enough large energy gap between the ^{3}*MLCT and ^{3}*MC states. Thus, further work seems to be necessary for any convincing explanation of the appearing issue. Until yet the most of the MLCT emitters analysed as descried above belong to the $c_{MLCT} > c_{LCT}$ class, only for very few examples reported in this work $c_{MLCT} \approx c_{LCT}$ could

Open Access Article. Published on 11 August 2020. Downloaded on 7/22/2024 10:31:27 PM.
This article is licensed under a Creative Commons Attribution-NonCommercial 3.0 Unported Licence.

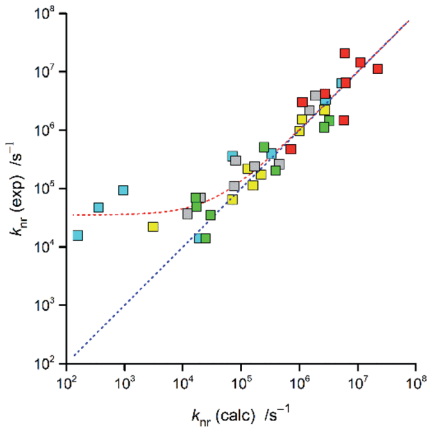

Fig. 7 Relationship between the calculated and experimentally found k_{nr} values for the $Re(CO)_2^+$ and $Re(CO)_3^+$ complexes. Data for $[Re(CO)_2(N^N)(tpp)_2]^+$ (yellow symbols), $[Re(CO)_2(N^N)(dppv)]^+$ (grey symbols),[20], $[Re(CO)_3(N^N)(tpp)]^+$ (cyan symbols), $[Re(CO)_3(N^N)(CH_3CN)]^+$ (green symbols),[12] and $[Re(CO)_3(N^N)(Cl)]$ (red symbols)[12] complexes in CH_3CN solutions at room temperature.

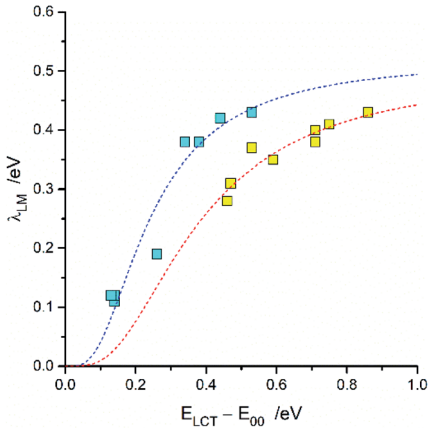

Fig. 8 Relationship between the λ_{LM} and $E_{LCT} - E_{00}$ terms for $[Re(CO)_2(N^N)(tpp)_2]^+$ (yellow symbols) and $[Re(CO)_3(N^N)(tpp)]^+$ (cyan symbols) complexes in CH_3CN solutions at room temperature. Dashed curves present fits according to eqn (7).

be anticipated (*vide infra*). Therefore, any more systematic data for the MLCT emitters with $c_{MLCT} < c_{LCT}$ would be particularly interesting.

For the complexes under study, the E_{00} energies found, as expected, depend on the nature of N^N ligand. Smaller E_{00} values are characteristic for the N^N ligands with stronger electron withdrawing properties. Generally, as it could be expected, the E_{00} values for the $[Re(CO)_3(N^N)(tpp)]^+$ complexes are larger (by *ca.* 0.30 eV) than those characterizing their $[Re(CO)_2(N^N)(tpp)_2]^+$ analogues. The fitted $h\nu_H$ values in the range of 0.15–0.23 eV correspond well to averaged contributions from the vibrational modes of the N=C, C=C, and C≡O bonds stretching in the N^N diimine (1200–1600 cm^{-1}) and CO (1850–2050 cm^{-1}) ligands, correspondingly. For the $[Re(CO)_2(N^N)(tpp)_2]^+$ complexes, the $h\nu_H$ values (0.15–0.20 eV) are somewhat smaller as compared with their $[Re(CO)_3(N^N)(tpp)]^+$ analogues (0.16–0.23 eV). In a similar way, the λ_H values (0.20–0.30 eV) found for the $[Re(CO)_3(N^N)(tpp)]^+$ complexes are somewhat larger than those characterizing their $[Re(CO)_2(N^N)(tpp)_2]^+$ counterparts (0.16–0.22 eV). One can tentatively attribute the observed differences in the fitted λ_H and $h\nu_H$ values to reorganization of two or three C≡O bonds. The found differences in the λ_H and $h\nu_H$ values explain the experimentally observed differences in the τ_{em} values for the $Re(CO)_2^+$ and $Re(CO)_3^+$ series. The longer τ_{em} values characteristic for the $Re(CO)_2^+$ complexes are evidently connected with suppression of the k_{nr} rate constants caused, in the way characteristic for the inverted Marcus region, by smaller λ_H and $h\nu_H$ values.

For both investigated series, the fitted λ_{LM} energies depend on the $E_{LCT} - E_{00}$ energy gap. The larger the $E_{LCT} - E_{00}$ term, the larger is the λ_{LM} value. The observed trends can be rationalized taking into account the electronic structures of the ^{3}*$[Re(CO)_2(N^N)(tpp)_2]^+$ and ^{3}*$[Re(CO)_3(N^N)(tpp)]^+$ emitters. The smaller the $E_{LCT} - E_{00}$ term, the larger contribution of the "pure" ^{3}*LC to the wave function of the given emitter is expected. Assuming that the λ_{LM} energy is mostly connected with the amount of the "pure" ^{3}*MLCT contribution to the observed "real" ^{3}*MLCT state, one can obtain the following expression

$$\lambda_{LM} = \lambda_{LM}^0 c_{MLCT}^4 = \lambda_{LM}^0 \frac{(E_{LCT} - E_{00})^2}{V_{33}^2 + (E_{LCT} - E_{00})^2} \quad (7)$$

where λ_{LM}^0 is the reorganization energy characterizing the "pure" ^{3}*MLCT state. The variability in the fitted values of the λ_{LM} energies, up to 0.15 eV for the $[Re(CO)_2(N^N)(tpp)_2]^+$ and up to 0.32 eV for the $[Re(CO)_3(N^N)(tpp)]^+$ series, is significantly more pronounced.

For the $[Re(CO)_2(N^N)(tpp)_2]^+$ and $[Re(CO)_3(N^N)(tpp)]^+$ series of the Re(I) complexes, the λ_{LM} values were fitted according to eqn (7) using λ_{LM}^0 and V_{33} as free fit parameters with obtaining good agreement between the experimental and fitted values (*cf.* Fig. 8). Whereas similar λ_{LM}^0 values, 0.52 and 0.50 eV are characteristic for the $[Re(CO)_3(N^N)(tpp)]^+$ and $[Re(CO)_2(N^N)(tpp)_2]^+$ series, the fitted V_{33} values (0.16 and 0.25 eV, respectively) are distinctly different. Such difference in the V_{33} values seems to be a general rule for the $Re(CO)_3^+$ and $Re(CO)_2^+$ complexes (*cf.* data in Table 3). The fits performed according to eqn (7) were done assuming V_{33} = const within the

Table 3 λ_{LM}^0 and V_{33} values obtained from the fits performed according to eqn (7)[a]

Complex series	λ_{LM}^0	V_{33}
$[Re(CO)_2(N^N)(tpp)_2]^+$	0.50	0.25
$[Re(CO)_2(N^N)(dppv)]^+$	0.48	0.26
$[Re(CO)_3(N^N)(Cl)]$	0.52	0.13
$[Re(CO)_3(N^N)(CH_3CN)]^+$	0.39	0.11
$[Re(CO)_3(N^N)(tpp)]^+$	0.52	0.16

[a] V_{33} and λ_{LM}^0 values for the $[Re(CO)_3(N^N)(Cl)]$, $[Re(CO)_3(N^N)(CH_3CN)]^+$, and $[Re(CO)_2(N^N)(dppv)]^+$ series obtained analysing previously published data.[12,20]

This journal is © The Royal Society of Chemistry 2020

Open Access Article. Published on 11 August 2020. Downloaded on 7/22/2024 10:31:27 PM.
This article is licensed under a Creative Commons Attribution-NonCommercial 3.0 Unported Licence.

given complex series. Thus, one should treat the obtained parameters fit parameters as an averaged V_{33} and λ^0_{LM} values.

Similarly to the observed variety of the λ_{LM} energies, one could expect the N^N ligand induced changes in the λ_H and $h\nu_H$ terms. Their values, however, depend rather weakly on the N^N ligand present in the emitters under study. One can rationalize the lack of the significant λ_H and $h\nu_H$ variation considering possible values of these parameters associated with the $S_0 \leftarrow {}^3$*LC emissions. For these emissions, with well-structured spectra, one can assume very small λ_{LM} and relatively large λ_H values. Then, independently of the c_{LCT} and c_{MLCT} coefficients attributed to the given MLCT emitter, the observed λ_H values should remain nearly constant. In an analogous way, this explains relatively small changes in the averaged high frequency intra-molecular vibrations.

The fitted λ_{LM} values contain contributions from the λ_L and λ_M reorganization energies. In a similar way, the λ_L and λ_M terms contributing to the overall λ_{LM} values are expected to follow analogous relationships. Separation of the both contributions is principally possible but requires some additional data and/or assumptions. Nominally, one can fit the emission band using more advanced model with two quantized modes corresponding to the medium ν_M and high ν_H frequency vibrations. However, since the one-mode approximation with expression (5) already gives a satisfactory agreement with experimental spectra the additional parameters do not follow from a free fit. Therefore, some of the fitting parameters (*e.g.*, medium ν_M and high ν_H frequencies) should be somewhat arbitrary fixed. Optionally, one can compare the λ_{LM} values at distinctly different temperatures (*e.g.*, 77 and 298 K) but this opportunity is not available for the investigated $[Re(CO)_3(N^N)(tpp)]^+$ complexes due to changes of their emission character, from the MLCT at 298 K to LC at 77 K. Such comparison, however, is possible for the $[Re(CO)_2(N^N)(tpp)_2]^+$ complexes exhibiting MLCT emission at both temperatures. This was performed in the manner as described previously for the $[Re(CO)_2(N^N)(dppv)]^+$ complexes[20] with finding the close analogy between both series of the $Re(CO)_2^+$ emitters.

The fitted V_{33} values together with the E_{00} energies provides some additional information about the nature of the given MLCT emitter allowing estimation of the c_{LCT} and c_{MLCT} coefficients. The c_{MLCT} coefficients calculated according to eqn (1) with the obtained V_{33} values comprise the ranges of 0.88–0.96 and 0.66–0.98 for the $Re(CO)_2^+$ and $Re(CO)_3^+$ series, respectively. This allows classifying nearly all the discussed complexes as the emitters with dominant MLCT nature. Only in some cases, namely the $[Re(CO)_3(N^N)(CH_3CN)]^+$ or $[Re(CO)_3(N^N)(tpp)]^+$ complexes bearing 47dmphen, 56dmphen or tmphen as N^N ligand, comparable contributions from the "pure" ^{3}*LC and ^{3}*MLCT excitations can be anticipated from the estimated c_{LCT} values. This remains in agreement with traces of the vibronic structures observed in the 298 K emission spectra of these complexes.

Nature of the lowest excited triplet state

DFT and TD-DFT computations were performed to obtain a deeper insight into the nature of the emissive ^{3}*$[Re(CO)_2(N^N)(tpp)_2]^+$ and ^{3}*$[Re(CO)_3(N^N)(tpp)]^+$ species. To attain more comparable results, additional computation performed for the all discussed series of the Re(I) complexes were done at the same level of theory. Geometries of the investigated complexes were optimized at the B3LYP level[57] for each stationary structure in the ground S_0 and the lowest triplet T_1 electronic states. Electronic transitions were calculated for the optimized structures using the TD-DFT method.[58] Calculation performed in CH_3CN solutions were done by means of the polarizable continuum solvation model.[59] Combination of Lanl2DZ basis set[60] (Re element) and the 3-21G* or 6-31G* basis sets (light elements) were employed in the present computations. Relatively small 3-21G* basis set was applied in the optimizations because, due to flexibility of tpp ligand, optimizations required much more computing time than it could be expected taking into account only number of atoms consisting the given tpp complex. The electronic transitions, however, were afforded using the Lanl2DZ and 6-31G* combination. Such approach was applied successfully for the heteroleptic Ru(II) and Os(II) complexes bearing α-diimine and phosphine ligands.[61] Our testing computations performed for selected $[Re(CO)_3(N^N)(Cl)]$ complexes provided results compatible with those presented in the literature.[62–65] This is particularly true for the shapes of the molecular orbitals and orbital assignment of the lowest excited states. In a similar way, agreement with the literature data for the $[Re(CO)_3(bpy)(tpp)]^+$ complex[66] was obtain.

The performed DFT and TD-DFT computations confirm the MLCT nature of the lowest triplet state anticipated for the discussed complexes. For the optimized T_1 geometry, the $S_0 \rightarrow T_1$ transitions are described mainly (with CI coefficients 0.66–0.69) between the HOMO and LUMO orbitals, localized on the Re(I) core and N^N ligand, respectively (*cf.* data in Table 3). All other computed quantities associated with the $S_0 \rightarrow T_1$ excitation confirm the MLCT nature of their lowest excited triplet state as well. Comparing the bond lengths computed for the optimized S_0 and T_1 states, one can see expected changes in the metal–ligands and intra-ligands bonds, *e.g.*, shortening of the Re–N bonds and elongation of the Re–P and Re–C bonds. This remains in accordance with increased positive charge on the central Re(I) ion. In a similar way, the computed changes in the C=N and C=C bond lengths are consistent with the introduction of an additional electron on the π* orbital of the N^N ligand. Congruently, the $S_0 \rightarrow T_1$ transitions lead to changes of the dipole moments characterizing the ground S_0 and the excited T_1 states. The observed lowering reflects well the charge redistribution associated with the MLCT excitation.

Analysis of the distribution of atomic charges and spin densities in the excited T_1 state of the discussed complexes supports intrinsic MLCT nature of these states. Upon inspecting the calculated spin densities for the investigated complexes, one can see that one of the unpaired electrons is localized mainly on the N^N ligand, whereas the second one on the remaining parts of the complexes. The observed *ca.* 1 : 1 spin redistribution symmetry is distinctly different from the 2 : 0 asymmetry expected for the ^{3}*LC excitation localized solely within the N^N ligand. For the discussed complexes, the 1 : 1

Open Access Article. Published on 11 August 2020. Downloaded on 7/22/2024 10:31:27 PM.
This article is licensed under a Creative Commons Attribution-NonCommercial 3.0 Unported Licence.

symmetry predictable for "pure" MLCT excitation is, however, to some extent broken. Whereas, the effect is relatively small for the investigated $Re(CO)_2^+$ complexes (*e.g.*, 1.13 : 0.87 for $[Re(CO)_2(bpy)(dppv)]^+$ chelate), the spin redistribution is distinctly more dissymmetric for $[Re(CO)_3(bpy)(tpp)]^+$ (1.22 : 0.78) or $[Re(CO)_3(bpy)(CH_3CN)]^+$ (1.31 : 0.69) complexes. The computation performed on the same level of theory gave for the prototype $[Re(CO)_3(bpy)(Cl)]$ complex nearly theoretical 1.04 : 0.96 ratio. Reasonably, larger spin redistribution dissymmetry arises from the DFT computation performed for other complexes under investigations. For example, the 1.49 : 0.51 and 1.31 : 0.69 ratios were found for the $[Re(CO)_3(47dmphen)(CH_3CN)]^+$ and $[Re(CO)_3(47dmphen)(tpp)]^+$ chelates. Noteworthy, the found differences in the spin redistribution extracted from the DFT computation follow adequately the c_{LCT} coefficients values that can be estimated using data the emission band-shape analysis. Using eqn (1) with affordable V_{33} and $E_{LCT} - E_{00}$ one can obtain the c_{LCT} values ranging from 0.15 to 0.71–0.75 for the $[Re(CO)_3(bpy)(Cl)]$ and $[Re(CO)_3(47dmphen)(CH_3CN)]^+$ or $[Re(CO)_3(47dmphen)(tpp)]^+$ complexes, respectively. For $c_{LCT} = 0.15$ one can expect the 1.02 : 0.98 spin redistribution ratio, whereas for $c_{LCT} = 0.75$ the 1.56 : 0.44 dissymmetry is anticipated. Thus, one can conclude nice congruence between the DFT and the band-shape analysis outcomes.

The obtained shapes of the molecular orbitals as well as the resulted orbital assignments of the low energy transitions remain in agreement with the MLCT nature of the low energy bands of the complexes under study. Shapes of their molecular orbitals (*cf.* Fig. 9) confirm metallic character of their HOMO, HOMO-1 and HOMO-2 levels involved in the low energy electronic transitions. The lowest LUMO orbitals participating in these transitions are essentially π* orbitals localized mainly on the N^N ligand with minor contributions from the Re(I) ion and other components forming the discussed complexes. However, although the HOMO, HOMO−1, and HOMO−2 possess mainly the metallic d orbital character, some contributions from the ligand attached to the Re(I) core are clearly seen. Thus, one can consider the low energy singlet and triplet states of the discussed complexes as the MLCT states with more or less

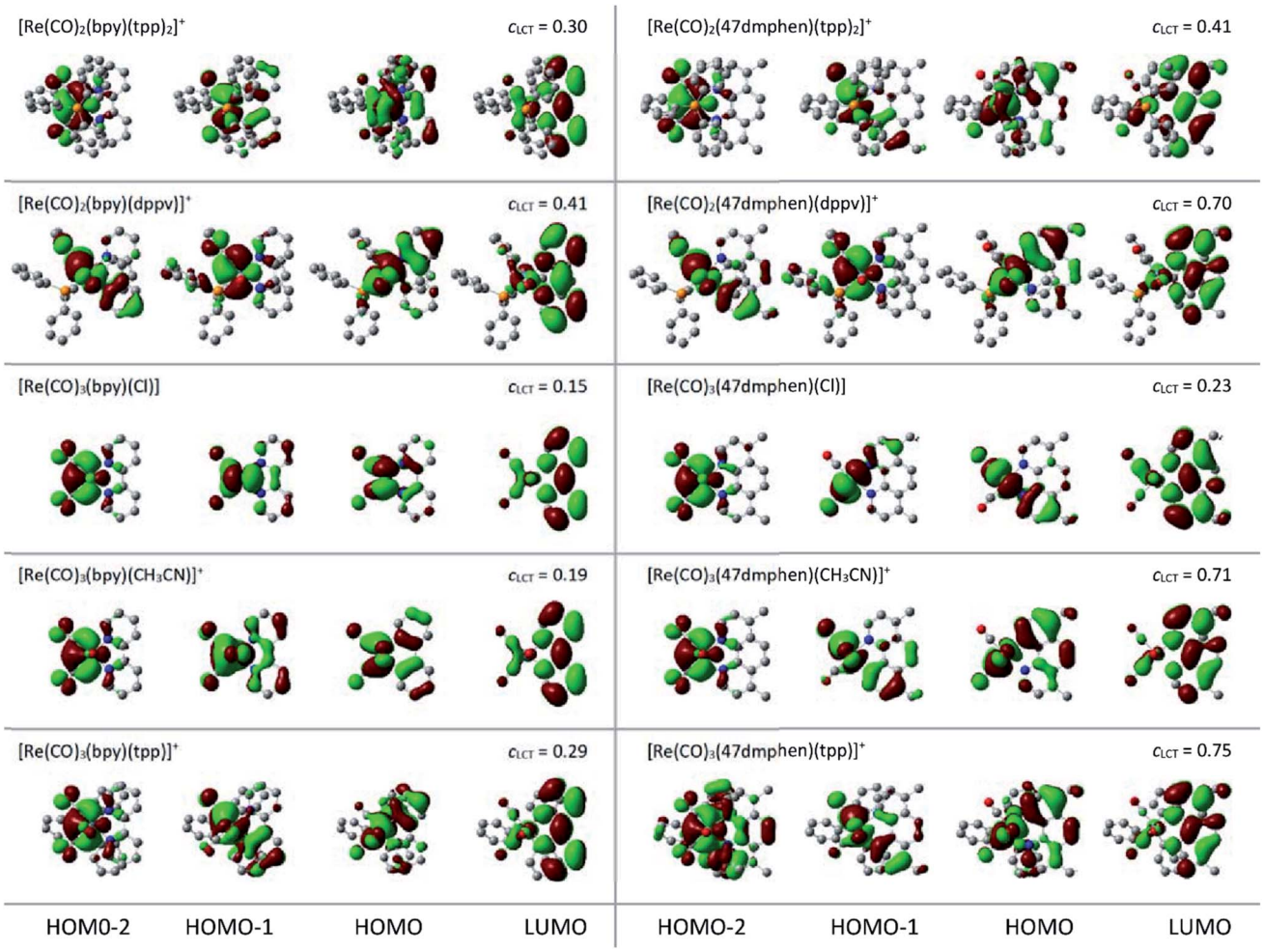

Fig. 9 Shapes of the frontier molecular orbitals for the bpy and 47dmphen complexes. Data (for CH_3CN solutions) from the TD-DFT computations performed for the lowest triplet states structures optimized in vacuum. Plots views (along *z*-axis) of the isodensity surfaces with contour value $Z = 0.02$.

 This journal is © The Royal Society of Chemistry 2020

Open Access Article. Published on 11 August 2020. Downloaded on 7/22/2024 10:31:27 PM.
This article is licensed under a Creative Commons Attribution-NonCommercial 3.0 Unported Licence.

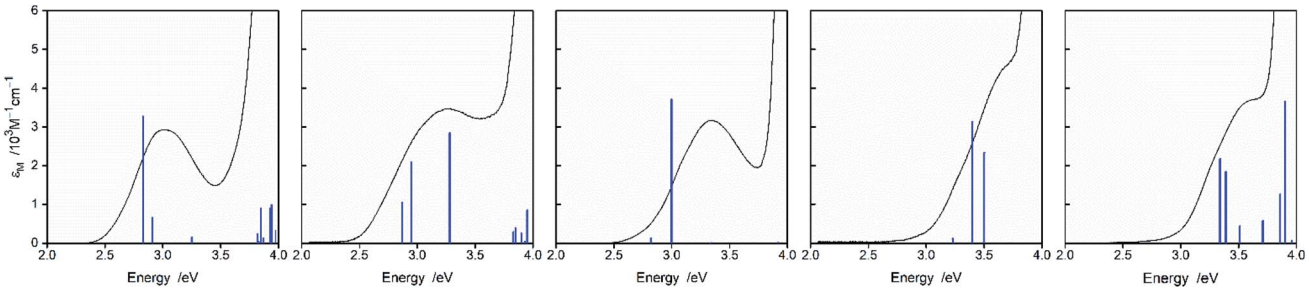

Fig. 10 MLCT parts of the UV-vis absorption spectra of the $[Re(CO)_2(bpy)(tpp)_2]^+$, $[Re(CO)_2(bpy)(dppv)]^+$, $[Re(CO)_3(bpy)(Cl)]$, $[Re(CO)_3(bpy)(CH_3CN)]^+$, and $[Re(CO)_3(bpy)(tpp)]^+$ complexes (from left to right) in CH_3CN solutions. Blue vertical bars correspond to the positions and relative intensities of the electronic transitions as obtained from TD-DFT computations.

pronounced admixture of the intra-ligand excitations. This is characteristic for the transitions within the singlet as well as the triplet manifolds. Moreover, both these excitation types should be treated as the charge-transfer between the whole $Re(CO)_3(tpp)^+$, $Re(CO)_3(CH_3CN)^+$, $Re(CO)_3(Cl)$, $Re(CO)_2(tpp)_2^+$ or $Re(CO)_2(dppv)^+$ fragments to the N^N ligand instead of somewhat oversimplified "pure" $d_{Re(I)} \rightarrow$ N^N or $d_{Re(II)} \leftarrow$ N^N$^-$ assignments.

Despite all found similarities, there are some intrinsic differences in properties of the discussed complexes. These include essential variety in the oscillator strengths of the computed vertical electronic transitions from the minima of the S_0 potential curves (*cf.* Fig. 10) as well from the S_0 states at the T_1 geometries, *i.e.*, at geometry of the Franck–Condon states reached in the $S_0 \leftarrow {}^3$*MLCT emissions (*cf.* data in Table 4). Such behaviour seems to be associated with different

Table 4 Energies E (in eV) and oscillator strengths f for the vertical electronic transitions with their orbital assignments.[a] Data (in CH_3CN solutions) from the TD-DFT computation performed for the S_0 states at geometries corresponding to the vacuum optimized structures of the lowest triplet state

Complex	$S_0 \rightarrow T_1$	$S_0 \rightarrow S_1$	$S_0 \rightarrow S_2$	$S_0 \rightarrow S_3$	$S_0 \rightarrow S_4$
$[Re(CO)_2(bpy)(tpp)_2]^+$	$E = 1.80$ 98% H/L	$E = 2.27, f = 0.103$ 99% H/L	$E = 2.63, f = 0.004$ 99% H−1/L	$E = 2.99, f = 0.011$ 99% H−2/L	$E = 3.44, f = 0.009$ 82% H/L+1 + 13% H−4/L
$[Re(CO)_2(bpy)(dppv)]^+$	$E = 1.85$ 94% H/L	$E = 2.29, f = 0.044$ 85% H/L+ 10% H−1/L	$E = 2.38, f = 0.010$ 89% H−1/L + 9% H/L	$E = 2.84, f = 0.076$ 93% H−2/L	$E = 3.38, f = 0.004$ 98% H/L+1
$[Re(CO)_3(bpy)(Cl)]$	$E = 1.92$ 92% H/L	$E = 2.10, f = 0.001$ 99% H/L	$E = 2.48, f = 0.077$ 98% H−1/L	$E = 2.77, f = 0.004$ 99% H−2/L	$E = 3.61, f = 0.001$ 87% H/L+1 + 11% H−3/L+1
$[Re(CO)_3(bpy)(CH_3CN)]^+$	$E = 2.09$ 78% H/L + 17% H−3/L	$E = 2.49, f = 0.000$ 99% H/L	$E = 2.80, f = 0.004$ 87% H−2/L + 12% H−1/L	$E = 2.95, f = 0.120$ 86% H−1/L + 12% H−2/L	$E = 3.76, f = 0.250$ 84% H−3/L + 11% H/L
$[Re(CO)_3(bpy)(tpp)]^+$	$E = 2.12$ 82% H/L	$E = 2.60, f = 0.049$ 93% H/L	$E = 2.93, f = 0.035$ 77% H−1/L + 18% H−2/L	$E = 3.02, f = 0.033$ 79% H−2/L + 16% H−1/L	$E = 3.36, f = 0.020$ 95% H−3/L
$[Re(CO)_2(47dmphen)(tpp)_2]^+$	$E = 1.81$ 92% H/L	$E = 2.45, f = 0.148$ 95% H/L	$E = 2.71, f = 0.032$ 81% H/L+1 + 13% H−1/L	$E = 2.75, f = 0.017$ 82% H−1/L + 16% H/L+1	$E = 3.10, f = 0.000$ 97% H−2/L
$[Re(CO)_2(47dmphen)(dppv)]^+$	$E = 1.84$ 90% H/L	$E = 2.58, f = 0.149$ 86% H/L + 7% H/L+1	$E = 2.67, f = 0.003$ 95% H−1/L	$E = 2.80, f = 0.038$ 88% H/L+1	$E = 3.05, f = 0.064$ 92% H−2/L
$[Re(CO)_3(47dmphen)(Cl)]$	$E = 1.98$ 87% H/L	$E = 2.45, f = 0.054$ 82% H/L	$E = 2.67, f = 0.069$ 81% H−1/L	$E = 2.82, f = 0.048$ 87% H/L+1	$E = 3.01, f = 0.009$ 60% H−2/L + 32% H−3/L
$[Re(CO)_3(47dmphen)(CH_3CN)]^+$	$E = 2.10$ 80% H/L	$E = 2.92, f = 0.072$ 69% H/L + 26% H−1/L	$E = 3.07, f = 0.092$ 69% H−1/L + 18% H/L	$E = 3.20, f = 0.005$ 91% H−2/L	$E = 3.30, f = 0.076$ 77% H/L+1, 9% H/L
$[Re(CO)_3(47dmphen)(tpp)]^+$	$E = 2.06$ 81% H/L	$E = 2.90, f = 0.181$ 92% H/L	$E = 3.14, f = 0.010$ 88% H−1/L + 11 H/L+1	$E = 3.23, f = 0.046$ 75% H/L+1 + 9% H−1/L	$E = 3.28, f = 0.008$ 60% H−2/L + 32% H−3/L

[a] H/L, H−1/L, H−2/L, H−3/L, H−4/L and H/L+1 denote HOMO → LUMO, HOMO−1 → LUMO, HOMO−2 → LUMO, HOMO−3 → LUMO, HOMO−4 → LUMO and HOMO → LUMO+1 transitions, respectively.

Open Access Article. Published on 11 August 2020. Downloaded on 7/22/2024 10:31:27 PM.
This article is licensed under a Creative Commons Attribution-NonCommercial 3.0 Unported Licence.

contributions of the individual Re(I) d orbitals to the molecular HOMO, HOMO−1, and HOMO−2 orbitals, respectively. Considering the shapes of the molecular orbitals involved in the individual transition, one can conclude that their symmetries are mainly responsible for the observed changes in the f patterns Nevertheless, the found sums of oscillator strengths f of the transitions with MLCT character remains (for the given N^N ligand) nearly constant over these chelates. The found small variety of the $\sum f$ values (*e.g.*, 0.08–0.12 for the bpy complexes) corresponds well with the observed similar values of the ε_m coefficients.

For all discussed Re(I) complexes the lowest $S_0 \rightarrow T_1$ transitions involve the HOMO and LUMO orbitals in accordance with their MLCT character. Energies of these transitions, computed at the lowest triplet state geometries, correspond quite well with the experimental $hc\tilde{\nu}_{em}^{max}$ values. Although the found agreement (*cf.* Fig. 11) could be somewhat better, one can regard the differences between experimental and computed values (up to *ca.* 0.3 eV) as acceptable taking into account low level of the theory. In similar way, the energies of the $S_0 \rightarrow {}^1$*MLCT transitions seem to be underestimated with comparable errors (*cf.* Fig. 10). Thus, one can conclude that the energy gaps between the lowest ^{3}*MLCT and ^{1}*MLCT states (ΔE_{ST}) available from the performed TD-DFT computations are, due to cancellation of possible errors, quite sensible values. One can also hypothesise that the TD-DFT energy gaps between T_1 and S_2 or T_1 and S_3 states are reasonable as well.

According to the data presented in Table 4, the computed ΔE_{ST} values, spanning the range from 0.18 to 0.84 eV, are much larger than one can expect taking into account only electronic interactions between the excited ^{3}*MLCT and ^{3}*LC states. In such a case, due to the electronic interactions within the ^{1}*LC/^{1}*MLCT and ^{3}LC/^{3}*MLCT manifolds, the initial degeneracy of the "pure" ^{1}*MLCT and ^{3}*MLCT states is removed. Thus, one can approximate the appearing energy splitting ΔE_{ST} between the "real" ^{1}*MLCT and ^{3}*MLCT states as follows:[20]

$$\Delta E_{MLCT} = \frac{V_{33}^2}{E_{LCT} - E_{00}} - \frac{V_{11}^2}{E_{LCS} - E_{00}} + \frac{V_{10}^2}{E_{00}} \quad (8)$$

where the V_{11} denotes the electronic coupling element responsible for the interactions between the initial ^{1}*MLCT and ^{1}*LC states, the latter characterized by the 0–0 transition energy E_{LCS}. Correspondingly, the electronic coupling element V_{10} describes the electronic interaction between the initial ^{1}*MLCT and the ground S_0 states with energy gap between them close to E_{00}. Due to expected similar values of the V_{11} and V_{10} terms as well as comparable values of the E_{00} and $E_{LCS} - E_{00}$ energy gaps, one can postulate cancelling of the contributions from the second and third terms in eqn (8) because they are working in the opposite directions. Thus, the first term on the right side of eqn (8) is dominantly contributing to the ΔE_{ST}:

$$\Delta E_{ST} = V_{33}^2/(E_{LCT} - E_{00}) \quad (9)$$

With the V_{33} and E_{00} quantities available from the emission band-shape analysis, one can estimate the ΔE_{ST} terms according to eqn (9). The resulting values, ranging from 0.02 to 0.25 eV, are up to nearly one order of magnitude smaller than the TD-DFT ones. Since such large discrepancy seems only hardly attributable to the possible errors in the V_{33} and E_{00} values, some other factors must affect the energy splitting between the lowest ^{3}*MLCT and ^{1}*MLCT states.

Comparing the ΔE_{ST} values estimated according to eqn (9) with those from the TD-DFT computations one can find significant correlation. The larger the c_{LCT} coefficient characterizing the given MLCT emitter, the larger is the observed discrepancy. This finding suggests important contributions from the exchange interactions between unpaired electrons of

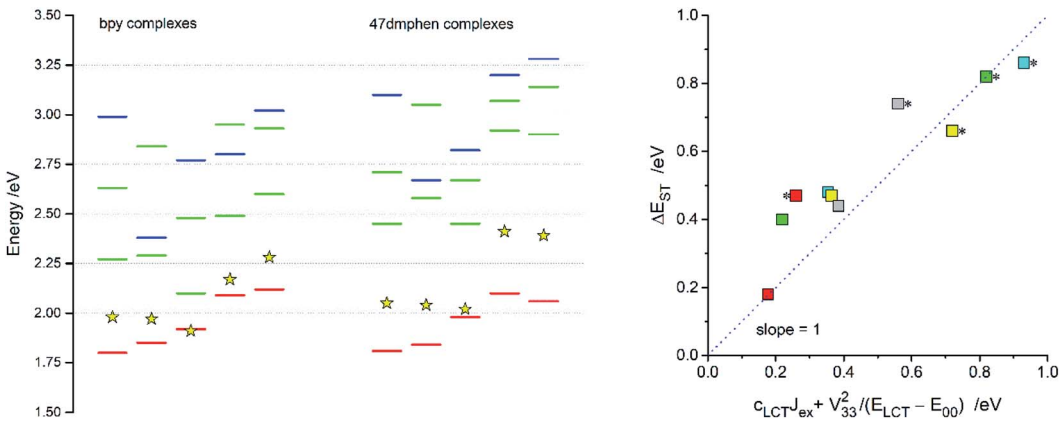

Fig. 11 TD-DFT energies of the $S_0 \rightarrow T_1$ (red bars) and $S_0 \rightarrow S_n$ transitions (green and blue bars) for the $[Re(CO)_2(N^N)(tpp)_2]^+$, $[Re(CO)_2(N^N)(dppv)]^+$, $[Re(CO)_3(N^N)(Cl)]$, $[Re(CO)_3(N^N)(CH_3CN)]^+$, $[Re(CO)_3(N^N)(tpp)]^+$ complexes (from the left to right). Data for the bpy (left column) and 47dmphen (right column) ligands. Blue bars indicate transitions from these HOMO−1 or HOMO−2 where their metallic character is connected with the Re(I) d_{xy} orbitals whereas green bars correspond to transitions from the HOMO, HOMO−1 or HOMO−2 originated from the d_{xz} and/or d_{yz} orbitals. Yellow star symbols denote the energies of the $S_0 \leftarrow {}^3$*MLCT emissions. Insert presents relation of the TD-DFT energy gaps ΔE_{ST} between the lowest excited ^{3}*MLCT and ^{1}*MLCT states to the ΔE_{ST} values calculated according to eqn (12). Data for the $[Re(CO)_2(N^N)(tpp)_2]^+$ (yellow symbols), $[Re(CO)_2(N^N)(dppv)]^+$ (grey symbols), $[Re(CO)_3(N^N)(Cl)]$ (red symbols), $[Re(CO)_3(N^N)(CH_3CN)]^+$ (green symbols), $[Re(CO)_3(N^N)(tpp)]^+$ (cyan symbols) complexes with 47dmphen (marked with * character) and bpy ligands.

 This journal is © The Royal Society of Chemistry 2020

Open Access Article. Published on 11 August 2020. Downloaded on 7/22/2024 10:31:27 PM.
This article is licensed under a Creative Commons Attribution-NonCommercial 3.0 Unported Licence.

the excited ^{3}*MLCT and ^{1}*MLCT states.[67,68] Thus, one can rationalize the observed ΔE_{ST} inconsistency taking into account the nature of the ψ_S and ψ_T wave functions of the lowest excited S_1 and T_1 states. If the S_1 state is nearly "pure" MLCT state, one can assume localization of the unpaired electrons mainly on the d and π^* orbitals. In such a case, with neglecting smaller contributions from other ligand or metal orbitals, one can express the ψ_S wave function as follows:

$$\psi_S = \psi_d + \psi_L \quad (10)$$

where ψ_d and ψ_L are the wave functions of the unpaired electrons localized on the d and π^* orbitals. The latter is the LUMO orbital of the N^N ligand. In the excited ^{3}*MLCT state the unpaired electrons are localized, due to mixing between "pure" ^{3}*LC and ^{3}*MLCT states, on the d, π and π^* orbitals. Thus, one can express the ψ_T wave function as follows:

$$\psi_T = c_{MLCT}\psi_d + c_{LCT}\psi_H + \psi_L \quad (11)$$

where ψ_H is the wave function describing the unpaired electrons localized on the π orbital (HOMO of the N^N ligand). Since the nature of the ψ_S and ψ_T wave functions determine the exchange energy, one can expect larger ΔE_{ST} values for the MLCT emitters with larger c_{LCT} coefficients. Searching of any connection between the TD-DFT results and the c_{LCT} and ΔE_{ST} parameters from the emission band-shape analysis, we have found following empirical relationship

$$\Delta E_{ST} = c_{LCT}J_{ex} + \frac{{V_{33}}^2}{E_{LCT} - E_{00}} \quad (12)$$

where J_{ex} is the energy exchange characterizing the given N^N ligand. Taking into account the respective J_{ex} values, 1.00 eV for 47dmphen[53] and 1.05 eV for bpy[55,69] ligands as determined from the fluorescence and phosphorescence spectra of their Zn(II) complexes, one can calculate the "theoretical" ΔE_{ST} values using eqn (12). Agreement between the TD-DFT values of the ΔE_{ST} energy gap with those calculated according to eqn (12) (*cf.* Fig. 11) can be regarded as more than satisfactory. Some deviations are explainable by errors in the analysed ΔE_{ST}, c_{LCT} and V_{33} values. Although Fig. 11 and Table 4 present data only for bpy and 47dmphen complexes, the found relationship seems to have a more general meaning. This conclusion arises from preliminary TD-DFT results obtained for some other $[Re(CO)_3(N^N)(CH_3CN)]^+$ and $[Re(CO)_3(N^N)(Cl)]$ complexes where the ΔE_{ST} *vs.* c_{LCT} relationship is fulfilled as well.

Transition dipole moments of $S_0 \leftarrow {}^3$*MLCT emission

The close analogy between complexes within the $Re(CO)_3^+$ and $Re(CO)_2^+$ series is also seen in the N^N ligand induced changes in the M_{em} values (*cf.* Fig. 12) where the M_{em} values are plotted against the $E_{LCT} - E_{00}$ difference. The applied correlation is based on our previous works,[12,20,29–31] where following relationship between the M_{em} and $(E_{LCT} - E_{00})/hc\tilde{\nu}_{em}^{max}$ was introduced

$$M_{em} = \frac{V_{10}V_{SOC}\Delta\mu}{{V_{33}}^2} \times \frac{E_{LCT} - E_{00}}{hc\tilde{\nu}_{em}^{max}} \quad (13)$$

where V_{SOC} is the spin–orbit coupling element between the lowest ^{3}*MLCT and ^{1}*MLCT states and $\Delta\mu$ is the difference in the dipole moments of the S_0 and "pure" ^{1}*MLCT states. Eqn (12) predicts linear correlation (with slopes equal to the $\chi_M = V_{10}V_{SOC}\Delta\mu/{V_{33}}^2$ terms) between the experimentally available M_{em} and $(E_{LCT} - E_{00})/hc\tilde{\nu}_{em}^{max}$ values when the remaining parameters are constant (or nearly constant) within analysed series of MLCT emitters. This may be expected when the coordinated N^N ligands are varied whereas the central metal ion and other coordinated ligands remain the same. The trend in the M_{em} values observed for the $[Re(CO)_2(N^N)(tpp)_2]^+$ series is similar to that found for the $[Re(CO)_2(N^N)(dppv)]^+$ one whereas the $[Re(CO)_3(N^N)(tpp)]^+$ complexes are more resembling their $[Re(CO)_3(N^N)(CH_3CN)]^+$ or $[Re(CO)_3(N^N)(Cl)]$ counterparts. The found χ_M slopes for the $Re(CO)_2^+$ series are distinctly smaller than those found for the $Re(CO)_3^+$ ones.

The above presented findings might suggest applicability of the eqn (12) in the quantitative interpretation of the experimentally found M_{em} values. Some fundamental reservations, however, allow regarding the observed coincidence as somewhat accidental. These arises because eqn (13) was derived assuming that the intensity borrowing from the lowest excited ^{1}*MLCT state is responsible for the radiative $S_0 \leftarrow {}^3$*MLCT deactivation. Then the transition dipole moment M_{em} is related to the ΔE_{ST} energy gap according to following relationship[70]

$$M_{em} = M_{01}V_{SOC}/\Delta E_{ST} \quad (14)$$

where M_{01} is the transition dipole moment of the $S_0 \leftarrow {}^1$*MLCT transition. Combining eqn (14) with eqn (9) and assuming that the M_{01} values follow the Hush-Mulliken formalism

$$M_{01} = \Delta\mu V_{10}/hc\tilde{\nu}_{em}^{max} \quad (15)$$

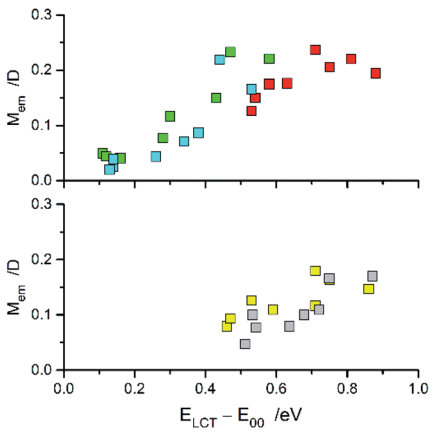

Fig. 12 Relationships between the M_{em} and $E_{LCT} - E_{00}$ quantities for the $Re(CO)_3^+$ (top) and $Re(CO)_2^+$ (bottom) complexes. Data for $[Re(CO)_2(N^N)(tpp)_2]^+$ (yellow symbols), $[Re(CO)_2(N^N)(dppv)]^+$ (grey symbols),[20], $[Re(CO)_3(N^N)(tpp)]^+$ (blue symbols), $[Re(CO)_3(N^N)(CH_3CN)]^+$ (green symbols),[12] and $[Re(CO)_3(N^N)(Cl)]$ (red symbols)[12] complexes in CH_3CN solutions at room temperature.

Open Access Article. Published on 11 August 2020. Downloaded on 7/22/2024 10:31:27 PM.
This article is licensed under a Creative Commons Attribution-NonCommercial 3.0 Unported Licence.

one can straightforwardly obtain eqn (13) which can be treated as the limiting $c_{\mathrm{MLCT}} \approx 1$ and $c_{\mathrm{LCT}} \approx 0$ case. Since in any more realistic situation $c_{\mathrm{MLCT}} < 1$ and $c_{\mathrm{LCT}} > 0$, one can correct eqn (13) taking into account eqn (12) with additional assumption that the effective spin–orbit coupling constants V_{SOC} depend on the c_{MLCT} coefficients as follows

$$V_{\mathrm{SOC}} = c_{\mathrm{MLCT}} V^0_{\mathrm{SOC}} \tag{16}$$

where V^0_{SOC} characterize the spin–orbit coupling between the "pure" ^{3}*MLCT and ^{1}*MLCT states. Then one can simply obtain following expression

$$M_{\mathrm{em}} = \frac{c_{\mathrm{MLCT}} V^0_{\mathrm{SOC}}}{c_{\mathrm{LCT}} J_{\mathrm{ex}} + {V_{33}}^2/(E_{\mathrm{LCT}} - E_{00})} \times \frac{V_{10}\Delta\mu}{hc\tilde{\nu}^{\max}_{\mathrm{em}}} \tag{17}$$

Since the c_{LCT} and c_{MLCT} coefficients are affordable from eqn (1) and typically $c_{\mathrm{LCT}} J_{\mathrm{ex}} \gg {V_{33}}^2/(E_{\mathrm{LCT}} - E_{00})$ one can further simplify eqn (17) to

$$M_{\mathrm{em}} = \frac{V_{10} V^0_{\mathrm{SOC}} \Delta\mu}{V_{33} J_{\mathrm{ex}}} \times \frac{(E_{\mathrm{LCT}} - E_{00})}{hc\tilde{\nu}^{\max}_{\mathrm{em}}} \tag{18}$$

The obtained expression, similarly to eqn (13), predicts again linear relationship between the experimentally determinable M_{em} and $(E_{\mathrm{LCT}} - E_{00})hc\tilde{\nu}^{\max}_{\mathrm{em}}$ quantities. Potentially one could apply eqn (18) in interpretation of the found similarities and variation of the experimentally found M_{em} values but some doubts appear concerning the spin–orbit coupling induced mixing of the lowest excited ^{3}*MLCT and ^{1}*MLCT states. This is because a ^{3}*MLCT state may couple effectively with a ^{1}*MLCT state if their electronic configurations involve the same π^* ligand orbital, but different d metal orbitals.[71,72] Thus, the required spin orbit coupling may be only weakly operative. Moreover, in the case of some α-diimine *fac*-$Re(CO)_3^+$ complexes, the oscillator strengths of their lowest $S_0 \rightarrow {}^1$*MLCT transitions (*cf.* data in Table 4) are very low, too low for an effective intensity borrowing responsible for the $S_0 \leftarrow {}^3$*MLCT emission.

Possible mixing between the lowest ^{3}*MLCT state with other singlet states may be treated as any plausible option explaining the experimentally observed M_{em} values. Then the resulting transition dipole moment M_{em} of the $S_0 \leftarrow {}^3$*MLCT emission can be expressed as follows[70]

$$M_{\mathrm{em}} = \sum_n \langle S_n|\mathbf{M}|S_0\rangle \frac{\langle S_n|\mathbf{V}_{\mathrm{SOC}}|T_1\rangle}{E(S_n) - E(T_1)} \tag{19}$$

where the $\mathbf{M}$ and $\mathbf{V}_{\mathrm{SOC}}$ are the dipole moment and the spin–orbit coupling operators, respectively. The $\mathbf{V}_{\mathrm{SOC}}$ operator mixes the lowest triplet state T_1 with energy $E(T_1)$ with the excited singlet states S_n with energies $E(S_n)$ whereas the $\mathbf{M}$ operator is responsible for the transition dipole moments of the spin allowed $S_0 \leftarrow S_n$ transitions. In the case of organometallic luminophore its ^{1}*MLCT states close in energy to the ^{3}*MLCT one are expected contributing mostly to the overall M_{em} value. This conclusion arises from relatively small energy gaps $E(^3\text{*MLCT}) - E(^1\text{*MLCT})$ and anticipated large values of the spin–orbit coupling constants. The latter is caused by the metallic character of the interacting ^{3}*MLCT and ^{1}*MLCT states. With this assumption, one can consider three excited ^{1}*MLCT state as potentially operative in the required intensity borrowing. Because one can exclude the electronic HOMO → LUMO transition from considerations, only the HOMO−1 → LUMO and HOMO−2 → LUMO transitions need more attention.

The perceived congruity between the band-shape analysis data and results from the performed TD-DFT computation allows considering the TD-DFT data as quite trustworthy. Thus, despite of low level of our computations, one can apply them to discuss the experimental M_{em} values in more details. Analysing the data collected in Table 4, however, it is rather difficult to find any simple correlation between the M_{em} and $\langle S_n|\mathbf{M}|S_0\rangle/[E(S_n) - E(T_1)]$ quantities. According to eqn (17) one can also expect (in some specific cases) the M_{em} values independent off the oscillator strengths redistribution over tree considered $S_0 \leftarrow {}^1$*MLCT transitions. However, this could be only possible when the numerators $\langle {}^1\text{*MLCT}_n|\mathbf{V}_{\mathrm{SOC}}|{}^3\text{*MLCT}\rangle$ in eqn (19) would be proportional to the denominators $E(^1\text{*MLCT}) - E(^3\text{*MLCT})$. Then, for all three conceivable contributions, the $V_{\mathrm{SOC}}/\Delta E$ terms remain constant and the resulting M_{em} values is simply proportional to the sum of $\langle {}^1\text{*MLCT}_n|\mathbf{M}|S_0\rangle$. Perhaps one can consider this special case as imaginable explanation of the experimental findings, but at the present stage of investigations, it remains as possible but very unlikely opportunity.

The second option is the intensity borrowing from the spin allowed $T_1 \rightarrow T_n$ transitions. In such a case, one can relate the M_{em} values to the spin–orbit induced coupling between the ground S_0 state and T_n states $\langle T_n|\mathbf{V}_{\mathrm{SOC}}|S_0\rangle$ and the transition dipole moments of the transitions $\langle T_n|\mathbf{M}|T_1\rangle$ occurring within the triplet manifold[70]

$$M_{\mathrm{em}} = \sum_n \langle T_n|\mathbf{M}|T_1\rangle \frac{\langle T_n|\mathbf{V}_{\mathrm{SOC}}|S_0\rangle}{E(T_n) - E(S_0)} \tag{20}$$

This option is, however, still less credible because the energy gaps $E(T_n) - E(S_0)$ are relatively large that should result in distinctly smaller V_{SOC} values. Because values of the $\langle T_n|\mathbf{V}_{\mathrm{SOC}}|S_0\rangle$ and $\langle S_n|\mathbf{V}_{\mathrm{SOC}}|T_1\rangle$ terms are anticipated to be similar, one could consider this option only for the $\langle T_n|\mathbf{M}|T_1\rangle$ values much larger than their $\langle S_n|\mathbf{M}|S_0\rangle$ complements. This is, however, very unlikely. Thus, one can expect potentially possible intensity borrowing from the $T_1 \rightarrow T_n$ transitions as rather small, most probably too small to explain the experimentally observed M_{em} values.

Finally, one can also consider a permanent dipole difference contribution arising from the direct spin–orbit coupling induced interactions between the ground S_0 and the excited ^{3}*MLCT states. Both involved states are metallic in their character that precludes possibly effective spin–orbit induced interactions between them. In this particular case the M_{em} values will depend on the differences between the dipole moments, $\mu(T_1)$ and $\mu(S_0)$, of the states involved in the $S_0 \leftarrow$

 This journal is © The Royal Society of Chemistry 2020

Open Access Article. Published on 11 August 2020. Downloaded on 7/22/2024 10:31:27 PM.
This article is licensed under a Creative Commons Attribution-NonCommercial 3.0 Unported Licence.

^{3}*MLCT transition and the spin–orbit coupling $\langle T_1|\mathbf{V}_{SOC}|S_0\rangle$ element responsible for interaction between them[70]

$$M_{em} = [\mu(T_1) - \mu(S_0)]\frac{\langle T_1|\mathbf{V}_{SOC}|S_0\rangle}{E(T_1) - E(S_0)} \quad (21)$$

One can attribute the energy gap $E(T_1) - E(S_0)$ in eqn (21) to the emission maxima $hc\tilde{\nu}_{em}^{max}$ of the given $S_0 \leftarrow {}^3$*MLCT transition. For both remaining terms, $\mu(T_1) - \mu(S_0)$ and $\langle T_1|\mathbf{V}_{SOC}|S_0\rangle$, one can expect their functional dependence on amount of the metallic character in the ^{3}*MLCT emitter. Both considered quantities depend on the value of the c_{MLCT} coefficient. Thus, the $\mu(T_1) - \mu(S_0)$ difference is approximately equal to $c_{MLCT}{}^2\Delta\mu$. Correspondingly, one can approximate the $\langle T_1|\mathbf{V}_{SOC}|S_0\rangle$ value as $c_{MLCT}V_{SOC}^0$. With the above remarks, one can simply obtain the following expressions

$$M_{em} = c_{MLCT}{}^3\frac{V_{SOC}^0\Delta\mu}{hc\tilde{\nu}_{em}^{max}} \quad (22)$$

According to eqn (22), one can anticipate the experimental M_{em} values related to the $c_{MLCT}{}^3$ factor. In fact a monotonic relationship between M_{em} and c_{MLCT} seems to be evident (*cf.* Fig. 13) but, instead of the expected $M_{em} \sim c_{MLCT}^3$ association, the M_{em} values can be linearized against $c_{MLCT}{}^9$. Similarly, as one can see in Fig. 12, the trends in the M_{em} values reflect the MLCT character of the given emitter. The experimental points are similarly scattered but the picture is more coherent, all five discussed Re(I) series follow the same layout. The larger the c_{MLCT} values in the ^{3}*MLCT state, the larger are the transition dipole moments attributed to the $S_0 \leftarrow {}^3$*MLCT emission. Evidently, the c_{MLCT} coefficient is the most important factor affecting the M_{em} values. Most probably, the higher MLCT characteristic involved in the singlet and triplet excited states, the spin–orbit coupling is more pronounced. Any exact origin of the observed correlation remains, however, an open question. Thus, one should treat the observed $M_{em} \sim c_{MLCT}{}^9$ relation as an empirical rule. On the other hand, similar correlations, *e.g.*, between the M_{em} and $(E_{LCT} - E_{00})/hc\tilde{\nu}_{em}^{max}$ values, have been found for in our previous works concerning some Os(II) or Ru(II) complexes.[29–31] Preliminary results from our investigations of the cyclometalated Ir(III) complexes $[Ir(C\hat{}N)_2(N\hat{}N)]^+$ suggests that these chelates follow the same trend as well. Thus, the correlations described in this work may have a general meaning and the problem is worthy for further investigations. To obtain an adequate solution, however, one can speculate that it will be necessary to go beyond simple perturbation theory. Very likely, a proper account of the spin–orbit coupling between the ground S_0 and the lowest ^{3}*MLCT states will require considerations of the spin-vibronic coupling.[73]

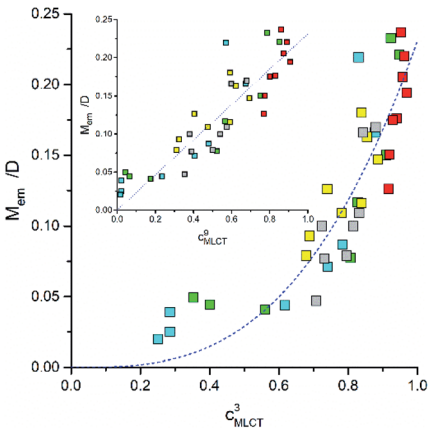

Fig. 13 Relationships between the M_{em} and c_{MLCT} quantities for the $Re(CO)_2^+$ and $Re(CO)_3^+$ complexes. Data for $[Re(CO)_2(N\hat{}N)(tpp)_2]^+$ (yellow symbols), $[Re(CO)_2(N\hat{}N)(dppv)]^+$ (grey symbols),[20], $[Re(CO)_3(N\hat{}N)(tpp)]^+$ (blue symbols), $[Re(CO)_3(N\hat{}N)(CH_3CN)]^+$ (green symbols),[12] and $[Re(CO)_3(N\hat{}N)(Cl)]$ (red symbols)[12] complexes in CH_3CN solutions at room temperature.

Concluding remarks

Comparative studies of the luminescence properties of $Re(CO)_2^+$ and $Re(CO)_3^+$ α-diimine chelates point to very similar nature of their lowest excited states. In both types of the complexes, their emissions in solutions at room temperature take place from the lowest excited T_1 states possessing distinct MLCT character. For most of the complexes discussed in this work, the 77 K emissions in solid matrices exhibit MLCT character as well. In some cases, however, the character of the 77 K emission change from MLCT to LC. Particularly well pronounced temperature effect can be seen for the $[Re(CO)_3(N\hat{}N)(tpp)]^+$ series where, independently of the coordinated N^N ligand, structured emissions have been recorded.

Despite all similarities, the investigated $Re(CO)_2^+$ and $Re(CO)_3^+$ complexes exhibit some important differences, particularly in the reorganization energies accompanying the electron transfer between the metallic center and the coordinated N^N ligand. Typically, the reorganization energies associated with high and low/medium frequency modes are distinctly smaller for the $Re(CO)_2^+$ complexes as compared to the $Re(CO)_3^+$ ones. This affects strongly the non-radiative deactivation of the excited ^{3}*MLCT states making the $Re(CO)_2^+$ chelates better emissive that is reflected in the higher emission quantum yields and longer emission life-times.

One can regard the reported complexes as well suited for the fundamental studies of the structure/properties relations for the MLCT emitters. In this work, two different approaches, analysis of emission band shapes and TD/TD-DFT computations, have been applied to clarify the observed changes in their luminescence properties as caused by the nature of the main and ancillary ligands. Well congruent results obtained from both applied methodologies shown that the data from band shape analyses are applicable in testing results from the quantum-mechanical computations, and *vice versa*. Particularly, both applied approaches point to crucial role of the lowest excited state ^{3}*LC localized within the coordinated N^N ligands. Mixing of the "pure" ^{3}*LC and ^{3}*MLCT configurations determines the nature of the given MLCT emitter affecting all quantities associated with the radiative as well as non-radiative $S_0 \leftarrow {}^3$*MLCT transitions.

Open Access Article. Published on 11 August 2020. Downloaded on 7/22/2024 10:31:27 PM.
This article is licensed under a Creative Commons Attribution-NonCommercial 3.0 Unported Licence.

Results from the performed band shape analyses of the $S_0 \leftarrow {}^3$*MLCT emissions have been applied in the interpretation of the experimentally determined rates of the non-radiative deactivations of the excited ^{3}*MLCT species. In most cases, the theoretically predicted k_{nr} values remain in nice agreement with those found experimentally. This confirms a close connection between the radiative and non-radiative deactivation of the excited states with the MLCT character. Intrinsic deviations between calculated and experimental k_{nr} values were, however, found for some of the MLCT emitters with large contributions of the ^{3}*LC excitation. Any more detailed explanation of this finding requires further systematic investigations.

Another unclear issue, origin of the electronic coupling between the lowest excited ^{3}*MLCT and the ground S_0 state requires further systematic investigations as well. The $S_0 \leftarrow {}^3$*MLCT transitions are, due to spin conservation rule, forbidden processes. They might become possible when the intensity borrowing through the spin–orbit coupling effects cause the mixing between the singlet and triplet states. Analysing the obtained TD-DFT data we are, however, not able to find any $S_0 \rightarrow S_n$ or $T_1 \rightarrow T_n$ transition responsible individually for the required intensity borrowing. At least not one which could be common for all five discussed series of Re(I) complexes with adequate explanation of the N^N ligand induced changes in the M_{em} values. Perhaps, one should treat each of the analysed MLCT emitters independently but this option seems to be improbable. The latter conclusion is based on the monotonic relationship between the M_{em} values and c_{MLCT} coefficients characterizing the MLCT character of the given MLCT emitter. Although the found $M_{em} \sim c_{MLCT}{}^9$ correlation looks somewhat amazing, this finding can have a more general meaning because similar behaviour is characteristic for other α-diimine complexes. At the present stage of investigations, however, it is rather difficult to provide any reliable explanation of these findings. Further work in such direction seems to be required for any decisive answer.

Experimental

Materials

Solvent used in UV-vis absorption and emission studies, acetonitrile – ACN, methanol, and ethanol, were of spectroscopic grade purchased from Aldrich. Reagents and analytical grade solvents, used without further purification in performed syntheses and purification of the investigated complexes, were purchased from Trimen, Acros Organics, Sigma-Aldrich or Alfa Aesar companies.

Both investigated series, $[Re(CO)_2(N^N)(tpp)_2]^+$ and $[Re(CO)_3(N^N)(tpp)]^+$, have been synthesized in the form of PF_6^- salts from $[Re(CO)_3(N^N)(Cl)]$ precursors[1,10,11] prepared according to well-known procedure reacting equimolar mixtures of $Re(CO)_5Cl$ and appropriate N^N ligand in refluxing toluene under argon for 4–5 h. The obtained precursors were further converted into $[Re(CO)_2(N^N)(tpp)_2]^+\cdots PF_6^-$ salts by refluxing their deoxygenated *o*-dichlorobenzene solutions containing $TlPF_6$ as dehalogenation agent and seven fold excess of tpp ligand for 2–4 h in dark.[16] After filtering of precipitated TlCl, the reaction mixture was cooled to room temperature and an excess of diethyl ether/hexane mixture was added to precipitate $[Re(CO)_2(N^N)(tpp)_2]^+\cdots PF_6^-$ products. The synthesized complexes were further purified by means of the column chromatography on activated acidic alumina with CH_2Cl_2/acetone 3 : 1 v/v mixture as eluent. The $[Re(CO)_3(N^N)(tpp)]^+\cdots PF_6^-$ salts[74] were prepared in a similar way using chlorobenzene as reaction medium. The reaction mixture was heated to 105–110 °C under argon in dark for 3 h. Due to the lower reaction temperature, refluxing of the deoxygenated chlorobenzene solutions containing equimolar amount of $[Re(CO)_3(N^N)(Cl)]$ and tpp with slight excess of $TlPF_6$ leads to $[Re(CO)_3(N^N)(tpp)]^+\cdots PF_6^-$ as main products. Column chromatography, performed on silica gel with $CHCl_3/CH_3OH$ 100 : 1 v/v as an eluent, resulted in final separation and purification of these complexes. Identification of all synthesized complexes was done by means of FT-IR, ^{31}P NMR and ^{1}H NMR spectroscopy. Acquired spectroscopic data confirm the expected structures of the synthesized complexes without any doubts. The recorded FT-IR spectra exhibit the presence of two (1919–1931 and 1830–1854 cm^{-1}) or three ((2027–2037, 1935–1954 and 1902–1935 cm^{-1}) sharp and intense absorption band in the $\nu_{C\equiv O}$ stretching region in accordance with the presence of two or three CO ligands in the $[Re(CO)_2(N^N)(tpp)_2]^+$ or $[Re(CO)_3(N^N)(tpp)]^+$ series, respectively. All the investigated complexes exhibit common features in their ^{31}P NMR spectra, exhibiting the presence of characteristic septet signals arising from the PF_6^- counterions ($\delta = -144.7$ ppm, $J \sim 706$ Hz). Additional singlet signals (with singlet-to-septet 2 : 1 or 1 : 1 intensity ratio) from the coordinated tpp ligands, in the range of 17–23 ppm for the $[Re(CO)_2(N^N)(tpp)_2]^+$ or 15–19 ppm for $[Re(CO)_3(N^N)(tpp)]^+$ series, correspond to the presence of two or one tpp ligand(s) in the analysed species. The presence of N^N and tpp ligands in these complexes is also nicely reflected in their ^{1}H NMR spectra where the integrated intensities of signals and their positions reproduce nicely the expected numbers of protons. Here the performed syntheses and identification of the synthesized complexes are only briefly mentioned. Any more detailed description will be reported elsewhere.

Instrumentation and procedures

FT-IR, ^{31}P and ^{1}H NMR spectra were acquired using Shimadzu IRAffinity-1 and VARIAN 400-MR spectrometers, respectively. UV-vis absorption spectra were measured using Shimadzu UV 3100 spectrophotometer, whereas corrected steady-state luminescence spectra and emission decays by means of Gilden Photonics FluoroSense and FluoroSense-P fluorimeters. In the case of emission studies, the investigated CH_3CN solutions were carefully deaerated by the prolonged saturation with preliminary purified and dried argon.

As a quantum yield standard, a solution of quinine sulphate in 0.1 N H_2SO_4 ($\phi_{ref} = 0.51$)[75] was used. The obtained emission quantum yields ϕ_{em} were measured with the estimated 10% accuracy. Emission spectra were fitted by means of a least-square method using OriginPro 9.0 software (Origin Lab Corp.) with user-defined functions. The experimental decay curves were analysed by the single-curve method using the

 This journal is © The Royal Society of Chemistry 2020

Open Access Article. Published on 11 August 2020. Downloaded on 7/22/2024 10:31:27 PM.
This article is licensed under a Creative Commons Attribution-NonCommercial 3.0 Unported Licence.

reference convolution based on the Marquardt algorithm.[76] with the χ^2 test and the distribution of residuals serving as the main criteria in the evaluation of fit quality. Emission lifetime τ_{em} values, characterizing the recorded decays were measured with the temporal resolution of *ca.* 0.01 μs. DFT and TD-DFT results presented in this work were obtained with the Gaussian software supported by GaussView 5.0.[77]

Conflicts of interest

There are no conflicts to declare.

Acknowledgements

This work is a part of the research project no. 24/20/B supported by the Siedlce University of Natural Sciences and Humanities.

References

1 M. Wrighton and D. L. Morse, *J. Am. Chem. Soc.*, 1974, **96**, 998.
2 R. A. Kirgan, B. P. Sullivan and D. P. Rillema, *Top. Curr. Chem.*, 2007, **281**, 45.
3 A. Kumar, S.-S. Sun and A. J. Lees, *Top. Organomet. Chem.*, 2010, **29**, 1.
4 H. Takeda, K. Koike, T. Morimoto, H. Inumaru and O. Ishitani, *Adv. Inorg. Chem.*, 2011, **63**, 137.
5 D. J. Stufkens and A. Vlcek Jr, *Coord. Chem. Rev.*, 1998, **177**, 127.
6 B. D. Rossenaar, D. J. Stufkens and A. Vlcek Jr, *Inorg. Chem.*, 1996, **35**, 2902.
7 L. Wallace, D. C. Jackman, D. P. Rillema and J. W. Merkert, *Inorg. Chem.*, 1995, **34**, 5210.
8 L. Sacksteder, M. Lee, J. N. Demas and B. A. DeGraf, *J. Am. Chem. Soc.*, 1993, **115**, 8230.
9 J. K. Hiño, L. Della Ciana, W. J. Dressick and P. Sullivan, *Inorg. Chem.*, 1992, **31**, 1072.
10 L. A. Worl, R. Duesing, P. Chen, L. Della Ciana and T. J. Meyer, *J. Chem. Soc., Dalton Trans.*, 1991, 849.
11 J. V. Caspar and T. J. Meyer, *J. Phys. Chem.*, 1983, **87**(6), 952.
12 A. Woźna and A. Kapturkiewicz, *Phys. Chem. Chem. Phys.*, 2015, **17**, 30468.
13 *Top. Curr. Chem.*, ed. V. Balzani and S. Campagna, 2007, vol. 280.
14 *Top. Curr. Chem.*, ed. V. Balzani and S. Campagna, 2007, vol. 281.
15 E. Schutte, J. B. Helms, S. M. Woessner, J. Bowen and B. P. Sullivan, *Inorg. Chem.*, 1998, **37**, 2618.
16 J. L. Smithback, J. B. Helms, E. Schutte, S. M. Woessner and B. P. Sullivan, *Inorg. Chem.*, 2006, **45**, 2163.
17 Y. Shen, B. Maliwal and J. Lakowicz, *J. Fluoresc.*, 2001, **11**, 315.
18 Y. Reece and D. G. Nocera, *J. Am. Chem. Soc.*, 2005, **127**, 9448.
19 H. Tsubaki, A. Sekine, Y. Ohashi, K. Koike, H. Takeda and O. Ishitani, *J. Am. Chem. Soc.*, 2005, **127**, 15544.
20 A. Kamecka, K. Prachnio and A. Kapturkiewicz, *J. Lumin.*, 2018, **203**, 409.
21 S. Sato and O. Ishitani, *Coord. Chem. Rev.*, 2015, **282–283**, 50.
22 C. D. Windle and R. N. Perutz, *Coord. Chem. Rev.*, 2012, **256**, 2562.
23 Q. Zhao, F. Li and C. Huang, *Chem. Soc. Rev.*, 2010, **39**, 3007.
24 K. K.-W. Lo, K. Y. Zhang and S. P.-Y. Li, *Eur. J. Inorg. Chem.*, 2011, 3551.
25 K. K.-W. Lo, *Acc. Chem. Res.*, 2015, **48**, 2985.
26 L. C.-C. Lee, K.-K. Leung and K. K.-W. Lo, *Dalton Trans.*, 2017, **46**, 16357.
27 G.-W. Zhao, J.-H. Zhao, Y.-X. Hu, D.-Y. Zhang and X. Li, *Synth. Met.*, 2016, **212**, 131.
28 Y. Yamazaki, H. Takeda and O. Ishitani, *J. Photochem. Photobiol., C*, 2015, **25**, 106.
29 A. Kamecka and A. Kapturkiewicz, *Phys. Chem. Chem. Phys.*, 2015, **17**, 23332.
30 A. Kamecka, K. Suwińska and A. Kapturkiewicz, *Phys. Chem. Chem. Phys.*, 2016, **18**, 28982.
31 A. Kamecka, V. Muszyńska and A. Kapturkiewicz, *J. Lumin.*, 2017, **192**, 842.
32 A. Ito and T. J. Meyer, *Phys. Chem. Chem. Phys.*, 2012, **14**, 13731.
33 Y. Shimura, *Bull. Chem. Soc. Jpn.*, 1988, **61**, 693.
34 P. Chen and T. J. Meyer, *Inorg. Chem.*, 1996, **35**, 5520.
35 R. A. Marcus, *J. Phys. Chem.*, 1990, **94**(12), 4963.
36 M. Bixon, J. Jortner and J. W. Verhoeven, *J. Am. Chem. Soc.*, 1994, **116**, 7349.
37 J. W. Verhoeven, T. Scherer, B. Wegewijs, R. M. Hermant, J. Jortner, M. Bixon, S. Depaemelaere and F. C. De Schryver, *Recl. Trav. Chim. Pays-Bas*, 1995, **114**, 443.
38 M. Senoue, T. Iwaki, K. Seki and M. Yagi, *J. Photochem. Photobiol., A*, 1996, **101**, 257.
39 M. A. A. Rashid, B. Saad, E.-S. M. Negim and M. I. Saleh, *World Appl. Sci. J.*, 2012, **17**, 958.
40 J. Higuchi, K. Suzuki, H. Arai, A. Saitoh and M. Yagi, *J. Phys. Chem.*, 1986, **90**, 1270.
41 R. A. Marcus, *J. Chem. Phys.*, 1956, **24**, 1261.
42 R. A. Marcus, *Annu. Rev. Phys. Chem.*, 1964, **15**, 155.
43 R. A. Marcus, *J. Phys. Chem.*, 1989, **93**, 3078.
44 *Electron Transfers – From Isolated Molecules to Biomolecules: Advances in Chemical Physics*, ed. J. Jortner and M. Bixon, vol. 106–107, Wiley, New York, 1999.
45 *Electron Transfer in Chemistry*, ed. V. Balzani, vol. 1, Wiley-VCH, Weinheim, 2001.
46 J. Cortes, H. Heitele and J. Jortner, *J. Phys. Chem.*, 1994, **98**, 2527.
47 J. Jortner, *J. Chem. Phys.*, 1976, **64**, 4860.
48 M. Bixon and J. Jortner, *J. Phys. Chem.*, 1991, **95**, 1941.
49 R. S. Mulliken, *J. Am. Chem. Soc.*, 1952, **74**, 811.
50 R. S. Mulliken, *J. Phys. Chem.*, 1952, **56**, 801.
51 N. S. Hush, *Prog. Inorg. Chem.*, 1967, **8**, 391.
52 N. S. Hush, *Electrochim. Acta*, 1968, **13**, 1005.
53 K. A. Walters, Y.-J. Kim and J. T. Hupp, *Inorg. Chem.*, 2002, **41**, 2909.
54 A. B. Maurer, E. J. Piechota and G. J. Meyer, *J. Phys. Chem.*, 2019, **123**, 8745.
55 J. V. Caspar and T. J. Meyer, *J. Am. Chem. Soc.*, 1983, **105**, 5583.

Open Access Article. Published on 11 August 2020. Downloaded on 7/22/2024 10:31:27 PM.
This article is licensed under a Creative Commons Attribution-NonCommercial 3.0 Unported Licence.

56 S. E. Angell, Y. Zhang, C. W. Rogers, M. O. Wolf and W. E. Jones Jr, *Inorg. Chem.*, 2005, **44**, 7377.
57 J.-F. Guillemole, V. Barone, L. Joubert and C. Adamo, *J. Phys. Chem. A*, 2002, **106**, 11354.
58 M. E. Casida, C. Jamorski, K. C. Casida and D. R. Salahub, *J. Chem. Phys.*, 1989, **108**, 4439.
59 S. Miertus, S. Scrocco and T. Tomasi, *Chem. Phys.*, 1981, **55**, 117.
60 P. J. Hay and W. R. Wadt, *J. Chem. Phys.*, 1985, **82**, 299.
61 Z.-Z. Xie and W.-H. Fang, *J. Mol. Struct.: THEOCHEM*, 2005, **717**, 179.
62 L. Yang, A.-M. Ren, J.-K. Feng, X.-J. Liu, Y.-G. Ma, M. Zhang, X.-D. Liu, J.-C. Shen and H.-X. Zhang, *J. Phys. Chem. A*, 2004, **108**, 6797.
63 R. Heydová, E. Gindensperger, R. Romano, J. Sýkora, A. Vlček Jr, S. Záliš and C. Daniel, *J. Phys. Chem. A*, 2012, **116**, 11319.
64 A. El Nahhas, C. Consani, A. M. Blanco-Rodríguez, K. M. Lancaster, O. Braem, A. Cannizzo, M. Towrie, I. P. Clark, S. Záliš, M. Chergui and A. Vlček Jr, *Inorg. Chem.*, 2011, **50**, 2932.
65 B. Machura, M. Wolff, M. Jaworska, P. Lodowski, E. Benoist, C. Carrayon, N. Saffon, R. Kruszynski and Z. Mazurak, *J. Organomet. Chem.*, 2011, **696**, 3068.
66 F. Zhao, J.-X. Wang, W.-Q. Liu and Y.-B. Wang, *Comput. Theor. Chem.*, 2012, **985**, 90.
67 B. J. Powell, *Sci. Rep.*, 2015, **5**, 10815.
68 A. C. Jacko, B. J. Powell and R. H. McKenzie, *J. Chem. Phys.*, 2010, **133**, 124314.
69 J. Kotlicka and Z. R. Grabowski, *J. Photochem.*, 1979, **11**, 413.
70 G. Baryshnikov, B. Minaev and H. Ågren, *Chem. Rev.*, 2017, **117**, 6500.
71 H. Yersin, *Highly Efficient OLEDs with Phosphorescent Materials*, Wiley-VCH, Weinheim, 2008.
72 E. Y.-T. Li, T.-Y. Jiang, Y. Chib and P.-T. Chou, *Phys. Chem. Chem. Phys.*, 2014, **16**, 26184.
73 T. J. Penfold, E. Gindensperger, C. Daniel and C. M. Marian, *Chem. Rev.*, 2018, **118**, 6975.
74 M. R. Gonçalves and K. P. M. Frin, *Polyhedron*, 2017, **132**, 20.
75 R. A. Velapoldi, in *National Bureau of Standards Special Publication 378, Accuracy in Spectrophotometry and Luminescence Measurements. Proc. Conf. NBS*, Gaithersburg, MD, 1972, p. 231.
76 D. W. Marquardt, *J. Soc. Ind. Appl. Math.*, 1963, **11**, 431.
77 M. J. Frisch, G. W. Trucks, H. B. Schlegel, G. E. Scuseria, M. A. Robb, J. R. Cheeseman, G. Scalmani, V. Barone, B. Mennucci, G. A. Petersson, H. Nakatsuji, M. Caricato, X. Li, H. P. Hratchian, A. F. Izmaylov, J. Bloino, G. Zheng, J. L. Sonnenberg, M. Hada, M. Ehara, K. Toyota, R. Fukuda, J. Hasegawa, M. Ishida, T. Nakajima, Y. Honda, O. Kitao, H. Nakai, T. Vreven, J. A. Montgomery Jr, J. E. Peralta, F. Ogliaro, M. Bearpark, J. J. Heyd, E. Brothers, K. N. Kudin, V. N. Staroverov, T. Keith, R. Kobayashi, J. Normand, K. Raghavachari, A. Rendell, J. C. Burant, S. S. Iyengar, J. Tomasi, M. Cossi, N. Rega, J. M. Millam, M. Klene, J. E. Knox, J. B. Cross, V. Bakken, C. Adamo, J. Jaramillo, R. Gomperts, R. E. Stratmann, O. Yazyev, A. J. Austin, R. Cammi, C. Pomelli, J. W. Ochterski, R. L. Martin, K. Morokuma, V. G. Zakrzewski, G. A. Voth, P. Salvador, J. J. Dannenberg, S. Dapprich, A. D. Daniels, O. Farkas, J. B. Foresman, J. V. Ortiz, J. Cioslowski and D. J. Fox, *Gaussian 09, Revision D.01*, Gaussian, Inc., Wallingford CT, 2013.

This journal is © The Royal Society of Chemistry 2020